JOURNAL OF GEOPHYSICAL RESEARCH, VOL. 111, C07011, doi:10.1029/2005JC003414, 2006

Click Here for Full Article

Mechanisms of decadal variability in the shallow subtropical-tropical circulation of the Atlantic Ocean: A model study

Sabine Hüttl[1] and Claus W. Böning[1]

Received 23 November 2005; revised 9 March 2006; accepted 10 April 2006; published 12 July 2006.

[1] A suite of basin-scale models of the thermohaline and wind-driven circulation in the Atlantic Ocean is used to study the mechanisms of decadal variability in the shallow subtropical-tropical cells (STCs). The emphasis is on the spatial patterns of the transport anomalies in the tropical thermocline, particularly their manifestation in the equatorial current system and on the relative role of changes in the deep meridional overturning cell (MOC) associated with variations in the formation of Labrador Sea Water (LSW) in the subpolar North Atlantic. Using wind stress and heat flux variations based on NCEP/NCAR-reanalysis products, the variability of the zonally integrated STC transports is similar to that obtained in a recent regional model study, corroborating the role of both the southern and northern STC in supporting wind-driven transport anomalies of O(2 Sv) near the equator. Sensitivity experiments indicate that changes in subarctic MOC transports associated with the strong variability in LSW formation during the last decades contributed a signal of O(0.3 Sv) to the upper-layer equatorial transports. Whereas the local wind-driven variability clearly dominates on interannual-decadal timescales and is confined to depths down to 150 m, the weak MOC-related signal is primarily reflected in an interdecadal modulation of the STC transports. While a strong part in the STC's transport anomalies is associated with the western boundary current (NBC), there is an important contribution also by weaker, interior ocean flow anomalies which tend to counteract the variability of the NBC.

Citation: Hüttl, S., and C. W. Böning (2006), Mechanisms of decadal variability in the shallow subtropical-tropical circulation of the Atlantic Ocean: A model study, *J. Geophys. Res.*, *111*, C07011, doi:10.1029/2005JC003414.

1. Introduction

[2] The upper-layer circulation in the western tropical Atlantic can be understood as a superposition of the northward, interhemispheric flow associated with the deep meridional overturning circulation (MOC), and the shallow subtropical-tropical circulation cells (STCs) connecting the subduction zones of the subtropical gyres with the equatorial regime of eastward currents [*McCreary and Lu*, 1994; *Liu et al.*, 1994; *Fratantoni et al.*, 2000]. Interest in the variability of the sub-surface, equatorward STC flows, stems from their role in both the physics and the biogeochemistry of the equatorial upwelling regimes in the eastern tropics: by providing extra-tropical, recently ventilated sources of relatively cold waters enriched in nutrients and oxygen, they represent the essential factors for both maintaining the sharp equatorial thermocline and the high biological productivity of this regime. While observational studies based on moored and ship-based current measurements along the western boundary have in recent years provided a fairly detailed account of the mean transports and their seasonal variability [*Schott et al.*, 2004], little is known as yet about the longer-term variability of this current system. In this study we aim to contribute to its understanding by evaluating a host of experiments with high-resolution models of the Atlantic Ocean, subject to varying wind stresses and heat fluxes based on reanalyses products for the period 1958–1999 (1/3-model version) and 1987–2003 (1/12-model version).

[3] A major consequence of the MOC which transports about 15 Sv of upper-layer water across the equator [*Ganachaud and Wunsch*, 2001], is a marked asymmetry in the strengths of the Atlantic STCs [*Fratantoni et al.*, 2000; *Jochum and Malanotte-Rizzoli*, 2001]. Observational evidence based on hydrographic data clearly indicates that the major contribution to the Equatorial Undercurrent (EUC) is of South Atlantic origin [*Metcalf and Stalcup*, 1967; *Tsuchiya*, 1986], with the equatorward flow mainly being carried along the western boundary by the North Brazil Undercurrent (NBUC [*Schott et al.*, 2002]), with some additional contributions from interior pathways [*Lazar et al.*, 2002; *Zhang et al.*, 2003]. The equatorward flow of North Atlantic thermocline water is comparatively weak, carried mostly off the western boundary by the Guyana Undercurrent [*Wilson et al.*, 1994; *Schott et al.*, 1998; *Bourles et al.*, 1999] and possibly

[1]Leibniz-Institut für Meereswissenschaften an der Universität Kiel, IFM-GEOMAR, Kiel, Germany.

Copyright 2006 by the American Geophysical Union.
0148-0227/06/2005JC003414$09.00

some additional, interior pathway [*Zhang et al.*, 2003] along the cyclonic geostrophic contours of the Guinea Dome area [*Stramma et al.*, 2005a]. The northern waters, however, do not appear to penetrate to the equator, but to join mainly the North Equatorial Countercurrent (NECC)/North Equatorial Undercurrent (NEUC)-system between 4°N and 8°N.

[4] The understanding of the physical mechanisms governing the mean pathways and transports in the tropical Atlantic has been aided by several ocean modeling studies. The salient features of the observational picture, particularly the predominantly southern origin of the EUC, and the dominance of the western boundary pathway for the equatorward flow of the South Atlantic water, are generally well reproduced in high-resolution models of the wind-driven and thermohaline circulation, such as the 1/4-OCCAM solution analyzed by *Hazeleger et al.* [2003], or the 1/3- and 1/12-FLAME cases described by *Böning and Kröger* [2005] and *Stramma et al.* [2005b]. A main area for quantitative differences between recent simulations has been the contribution of the northern STC, suggestive of the sensitivity of this feature to the strength of the MOC. *Fratantoni et al.* [2000] and *Jochum and Malanotte-Rizzoli* [2001] showed a strengthening/weakening of the northern STC in the case of a weak/strong meridional overturning. A main effect of the upper-layer MOC flow is to inhibit the northern hemisphere exchange between subtropics and tropics near the western boundary. The interior exchange window on the northern hemisphere is blocked by the high PV-ridge created by the ITCZ [*Zhang et al.*, 2003] and is sensitive to the applied wind forcing [*Inui et al.*, 2002].

[5] Differences in the strength of the MOC were found to be manifested in the western boundary currents, with a weaker MOC being reflected in a weaker NBUC/NBC-system (as exemplified in the ''DYNAMO'' model intercomparison [*Barnier et al.*, 2001]) and a more intense Guyana Undercurrent (as in the ''CME'' model cases analyzed by *Schott and Böning* [1991]). However, despite such differences in the mean fields, certain aspects of the seasonal cycle (i.e., the integral transports of mass and heat) in the tropical Atlantic appeared rather robust across various models, with high-resolution solutions also exhibiting a fair quantitative reproduction of the observed, temporal and spatial characteristics of the seasonal current variability at the western boundary [*Böning and Kröger*, 2005] and on the equator [*Thierry et al.*, 2004; *Brandt and Eden*, 2005].

[6] While observational studies using moored current meters and repeated ship-based velocity profiling and altimetry [cf. *Brandt and Eden*, 2005] have allowed quantitative estimates for the annual mean transports and their annual cycle near the western boundary [*Bourles et al.*, 1999; *Johns et al.*, 1998; *Schott et al.*, 1998, 2002, 2003], there is as yet little knowledge in contrast to the Pacific [e.g., *McPhaden and Zhang*, 2002] about the longer-term variability of the Atlantic STCs and their possible relation to the observed decadal variability in the tropical SST [*Schott et al.*, 2004]. The question of an active ocean's role in tropical Atlantic climate variability, of importance especially in the context of a potential predictability, has hence been addressed mainly through modeling studies of the ocean-atmosphere system. Concerning tropical SST variability off the equator, the focus has particularly been on the inter-hemispheric gradient of anomalous SST which influences the seasonal migration of the ITCZ and is thus related to rainfall anomalies over northeastern Brazil [*Hastenrath and Greischar*, 1993]. In model studies the off-equatorial SST variability was found to be primarily governed by low-frequency changes in evaporation associated with anomalies in the local trade winds [*Carton et al.*, 1996]. The influence of ocean heat transport remains controversial: studies showed it either of little influence [*Dommenget and Latif*, 2000], or to act as a damping term opposing the effect of latent heat flux anomalies [*Seager et al.*, 2001], but also proposed it to play a more fundamental, active role in the generation of decadal SST anomalies [*Chang et al.*, 2001].

[7] Near the equator the strongest variations of SST (sometimes referred to as Atlantic Ninos) occur in the eastern ocean, associated with anomalous vertical displacements of the thermocline [*Carton et al.*, 1996], with important local climate effects along the coastal zone of tropical Africa [e.g., *Hisard*, 1980; *Carton and Huang*, 1994]. The model study by *Carton et al.* [1996] showed this variability, in contrast to the off-equatorial mode, dominated by dynamical processes: in their investigation of the relative importance of heat flux and momentum forcing (based on COADS fields for 1960–1989) in a regional ocean model of medium ($0.5° \times 1.5°$) resolution, most SST variability in the eastern Atlantic resulted from wind anomalies within ±7.5° of the equator, involving a transport of heat anomalies from the western basin, supplied from either the northwestern or southwestern tropical ocean.

[8] The forcing mechanisms of decadal SST anomalies in the equatorial Atlantic have recently been elucidated further by *Kröger et al.* [2005], using a reduced-gravity model for the Atlantic Ocean between 40°S and 40°N (with a resolution of 1/2° in longitude and a stretched grid in latitude, with 1/3° within 10°S–10°N), coupled to an advective atmospheric mixed layer model, subject to NCEP wind fields for 1948–2001. The MOC was mimicked by restoring to climatological hydrographic conditions near the northern and southern boundaries, leading to a cross equatorial flow of about 12 Sv. A suite of sensitivity experiments showed that the decadal response of the equatorial SST, although being dominated by local dynamical forcing, nevertheless involved a weak, but significant part associated with remote, subtropical forcing (i.e., between 5° and 15° latitude) and an oceanic bridging by the equatorward flows of the STCs. A similar finding, of an off-equatorial effect on ENSO-decadal variability, was reported by *Nonaka et al.* [2002] for the Pacific Ocean. An interesting aspect of the solution was that, despite the north-south asymmetry in the mean transports, both the southern and the northern STCs were important in producing equatorial SST anomalies due to wind changes at higher latitudes. Whereas the northern hemisphere effect on modulating equatorial SST variability was dominated by wind-driven changes in the strength of the STC (commonly referred to as the $v'\bar{T}$-mechanism [*Kleeman et al.*, 1999]), the southern hemisphere involved both this process as well as some effect due to equatorward advection of temperature anomalies by the mean flow in the subtropical thermocline (the $\bar{v}T'$-mechanism, originally proposed by *Gu and Philander* [1997]). Regarding the latter mechanism, *Lazar et al.* [2001], in their model investigation of the propagation processes involved in the

spreading of an idealized temperature anomaly (of 2.2°C) inserted into the subduction area of the eastern subtropical South Atlantic, also noted a weak (of about 0.2°C) effect after 6–8 years in the equatorial thermocline.

[9] Another remote forcing mechanism, potentially capable of inducing tropical variability, but usually excluded in studies based on regional models with climatological inflow conditions at the lateral boundaries, involves anomalies of the deep MOC. A possible candidate for generating decadal MOC variations, first proposed by *Yang* [1999], is the formation rate of Labrador Sea Water (LSW) through deep winter convection, which is subject to strong changes due to the variability of the air-sea fluxes associated with the North Atlantic Oscillation (NAO [*Curry et al.*, 1998]). However, while observational estimates indicate a decadal range of LSW formation of about 10 Sv [*Marsh*, 2000; *Rhein et al.*, 2002], little is known as yet about the dynamical response of the MOC transport apart from model studies. Ocean models forced by reanalysis fluxes [*Häkkinen*, 1999; *Eden and Willebrand*, 2001; *Beismann and Barnier*, 2004; *Bentsen et al.*, 2004] consistently show an increase of the MOC at mid-latitudes by about 20% of its mean, from lowest values during the 1960s or early 1970s, to a maximum in the mid-1990s. While transport anomalies of subarctic origin extend quite rapidly, albeit attenuated, to the equator by fast wave processes along the western boundary [*Getzlaff et al.*, 2005], the effect of the ensuing, relatively small changes in the equatorial MOC transport on the upper-layer tropical variability has remained controversial. *Yang* [1999] noted a correlation between LSW thickness and the interhemispheric difference of SST in the tropical Atlantic with a lag of 5 years, a pattern of response consistent with an idealized model simulation. A recent study by *Zhang and Delworth* [2005] also shows a strong response on decadal scales of the coupled ocean-atmosphere system to changes in the North Atlantic freshwater balance: they show that enhanced freshwater forcing leads to a southward shift of the ITCZ in the tropical Atlantic and Pacific and consequently to a tropical dipole anomaly with a cooling on the northern and a warming of the southern hemisphere.

[10] The objective of the present paper is to advance the understanding of the tropical Atlantic's response to atmospheric forcing variability, focusing on the induced variability of the STC-related flow fields in a sequence of high-resolution, basin-scale models. The perspective provided is in some sense complementary to previous studies, in that the prime concern here is not on the issue of the role of ocean dynamics in the generation of tropical SST anomalies. By focusing on the low-frequency flow patterns in the western equatorial Atlantic, in a model capable of resolving the salient characteristics of the observed current fields, our analysis instead aims at elucidating aspects of the STC variability that are relevant particularly in the context of potential monitoring systems.

[11] The questions addressed in this regard include the following: (1) How robust are the (integral) patterns and amplitudes of STC variability as, e.g., reported in the regional model study of *Kröger et al.* [2005]? (2) What is, under realistic forcing conditions, the significance of a MOC signal of subarctic origin in the tropical Atlantic, and what timescales are involved in this response? (3) What is the manifestation of variations in the zonally integrated STC transports near the western boundary: i.e., to what extent could the STC variability be captured by transport records obtained in the boundary current system?

2. Model and Data

[12] Our experiments are based on a hierarchy of primitive equation models that has been developed for studying the wind-driven and thermohaline circulation in the Atlantic Ocean (Family of Atlantic Model Experiments, FLAME); the present study specifically builds on previous applications of the FLAME system to issues of the seasonal variability in the tropical Atlantic [*Böning and Kröger*, 2005; *Brandt and Eden*, 2005], of the decadal variability in the formation of LSW and in the MOC [*Eden and Willebrand*, 2001; *Böning et al.*, 2003] and the associated propagation of a MOC signal to the tropics [*Getzlaff et al.*, 2005]. The z-coordinate model is based on a modified version of the Modular Ocean Model (MOM2 [*Pacanowski*, 1995]). All model cases described here use 45 levels in the vertical, with a 10 m-resolution at the surface, smoothly increasing to a maximum of 250 m below 2250 m. Vertical mixing is parameterized based on the stability-dependent scheme for vertical diffusivity (κ_h = 0.1–4.0 cm^2/s) and viscosity (κ_m = 2.0–10.0 cm^2/s) as described in more detail by *Böning and Kröger* [2005], and a KT-scheme [*Kraus and Turner*, 1967] for the mixed layer. The subgrid-scale lateral mixing is parameterized by a harmonic operator on isopycnals (A_h = 2.0*10^6 cm^2/s). (Note: *Böning and Kröger* [2005] and *Kröger* [2001] showed in a regional model configuration of FLAME that a biharmonic mixing formulation permits a more detailed equatorial current system at 1/3 resolution. The present choice compromises the fidelity of the 1/3-cases in this regard, but is motivated by the need to capture aspects of the basin-scale overturning and deep water formation at high latitudes, essential to one of our questions. The effect of an improved resolution of the zonal current system is addressed by the 1/12-case.

[13] The main model experiments discussed here cover the Atlantic Ocean between 70°N and 70°S, 100°W and 30°E, adopting an ''eddy-permitting'', locally isotropic (Mercator) grid with longitudinal (latitudinal) sizes of 1/3° (1/3° × cosϕ)). The model was spun up for 57 years using a repeated annual cycle of atmospheric forcing as in the ''DYNAMO'' model intercomparison [*Willebrand et al.*, 2001; *Barnier et al.*, 2001] and as in the previous study of *Böning and Kröger* [2005], based on the monthly mean wind stresses and linearized bulk heat fluxes as derived from ECMWF analyses for the years 1986–1988 by *Barnier et al.* [1995]. The northern and southern boundaries are closed, with a damping of T and S towards climatological hydrographic conditions: at the northern boundary using those developed by *Dynamo Group* [1997], at the southern boundary using a combined data set from *Boyer and Levitus* [1997] and *Levitus and Boyer* [1994]. Note, that the restoring at the northern boundary effectively inhibits an interannual variability of the overflow water masses, so we are able to study the effects of subarctic variability in separation. For the western and eastern boundaries in the south there is a prescribed in- and outflow of the ACC.

[14] Following the spin-up period, a sequence of experiments was performed to study the ocean's response to

interannually varying atmospheric forcing, based on the NCEP/NCAR-reanalyses [*Kalnay et al.*, 1996] for 1958–1999. (In order to avoid a distortion of the model's mean state, NCEP-anomalies were combined with the climatological fields from the ECMWF used for the spin-up). The specification of the thermal forcing follows the linearized bulk formulation of air-sea flux variability introduced by *Eden and Willebrand* [2001] which revealed a realistic depiction of observed LSW signatures [*Böning et al.*, 2003]. It has to be noted that while this bulk heat flux formulation appears a useful choice for examining the spreading of high-latitude transport signals into the tropical Atlantic, it lacks physical processes that seem to be relevant for the generation of decadal SST variability in the tropical Atlantic [*Seager et al.*, 2001]: i.e., the specification of the atmospheric state implied by the heat flux formulation inhibits the possibility of air-sea interactions such as the wind-evaporation effect discussed by *Chang et al.* [1997] and *Kushnir et al.* [2002], and may thus overestimate the damping effect of the local heat flux on SST anomalies.

[15] Our main experiment (at 1/3° resolution) includes interannual wind stress and heat flux forcing and is referred in the following as Exp. 1. To resolve the effect of resolution there is a shorter-period integration of a 1/12°-version (Exp. 2) of FLAME, i.e., a spin-up of 9 years under climatological forcing, followed by an interannually forced period from 1987–2003. We use the same kind of forcing as for the 1/3°-model to assess robustness of the transport variability and to study the impact of better resolving the current structures.

[16] In order to differentiate between the impact of forcing components, the main experiment is complemented by a second 1/3° experiment (Exp. 3) where the interannual variations in wind stresses are switched off. While previous studies of the causes of STC variability have clearly shown the dominance of dynamical (wind stress) generation mechanisms [e.g., *Kröger et al.*, 2005], Exp. 3 will provide, in particular, a clearer perception of the relative importance of remotely generated variability, i.e., of the MOC signal associated with LSW formation variability. Note that Exp. 3 is the same as used in the previous studies of LSW formation variability [*Böning et al.*, 2003] and the equatorward propagation of the associated MOC anomalies [*Getzlaff et al.*, 2005]. To examine the remote effect of the LSW-induced changes in the MOC in isolation, an additional sensitivity run was performed. In this case (Exp. 4), LSW formation was permanently suppressed by preventing sea surface temperatures below 5°C in the Labrador Sea region, thereby effectively eliminating deep winter convection and a renewal of LSW. The response to this perturbation will be studied in section 4.3.

3. Mean Circulation and Annual Cycle

[17] It is useful to precede the discussion of the low-frequency variability by an examination of the mean current patterns comprising the subtropical-tropical exchange regime. We will thus provide an analysis of the pathways and transports of the equatorward flows in the thermocline, and their connection with the equatorial upwelling regime and as a prerequisite for the discussion of the interannual variability (sect. 4), also a brief examination of the seasonal cycle which constitutes a vigorous signal in the equatorial Atlantic. A comparison with observational records in this regard will allow some assessment of the ability of the model to simulate aspects of the wind-driven variability.

3.1. Annual Mean

[18] Since the structure of the STCs and, accordingly, the intensity of the tropical current system in the Atlantic is strongly affected by the cross-equatorial transports associated with the southward export of NADW, it is useful to begin with an examination of the zonally integrated transports for both the upper- and deep-layers of the tropical Atlantic. Figure 1 depicts a net southward flow of deep water of 15 Sv for the 1/3°- (Figure 1a) and 16 Sv for 1/12°-model cases (Figure 1b), in accordance with recent inversions (16 Sv) of hydrographic section data by *Lumpkin and Speer* [2003]. About two-thirds of the corresponding northward flux in the upper 1000 m are entrained into the equatorial upwelling system. This supply of source waters of extra-tropical southern hemispheric origin roughly matches the northward transport across 10°N of about 9 Sv (10 Sv for the 1/12 case) in the surface (Ekman) layer; this northward MOC flow extending into the depth range of the equatorward branch of a possible northern STC (nSTC) prevents such a cell on the northern hemisphere. The southern STC (sSTC) can be identified with a northward transport (at 5°S to 10°S) of 6 Sv in Exp. 1 and 8 Sv in Exp. 2 in Figures 1a and 1b between 0 and 300 m. The equatorward flow can be understood to consist of two components: an upper part associated with the wind-driven sSTC (negative values of the stream function in Figures 1a and 1b, upper 100 m) and a part of the MOC return flow, below $\approx$100 m/σ_θ = 25.3 kg/m^3 and above 300 m/σ_θ = 26.2. Both portions contribute to the upwelling into the surface layer (roughly defined here as the upper 20 m) at the equator. In the discussion of the variability of STC or NBC we will hence calculate transports above 300 m depth. Specifically the transport of the NBC will be calculated as the northward flow between the western boundary and 33°W, from 20 m to 300 m depth, thereby excluding the surface (Ekman) flow to the south. To calculate thermocline transports for Exp. 1 and 3 we integrate between the isopycnals σ_θ = 24.4–26.2 kg/m^3, as Figure 1c indicates. The EUC is calculated in the same depth or density range and is defined as the eastward flow between 3°S and 3°N.

[19] The upwelling transport into the surface layer (above 20 m) between 10°S and 10°N, associated with the wind-driven equatorial Ekman divergence, is about 14 Sv for the 1/3°-, and about 15 Sv for the 1/12°-model (due to more eddy activity and recirculation in the 1/12° model), respectively. These values appear very close to the estimate of the Ekman divergence between 35°W and 4°W (15 Sv) by *Gouriou and Reverdin* [1992], but are significantly lower than values inferred from NCEP reanalysis stresses (26 Sv) by *Schott et al.* [2004]; higher values (21 ± 2.1 Sv) are also reported by *Zhang et al.* [2003] based on surface drifter data between 6°S and 10°N. Note, however, that values for the equatorial upwelling/divergence are very sensitive to the latitudinal range considered: e.g., in the narrow band of 2°S to 2°N, there is an upwelling of 23 Sv, similar to that found by *Hazeleger et al.* [2003] for the OCCAM model in this area. A significant part of this equatorial upwelling is

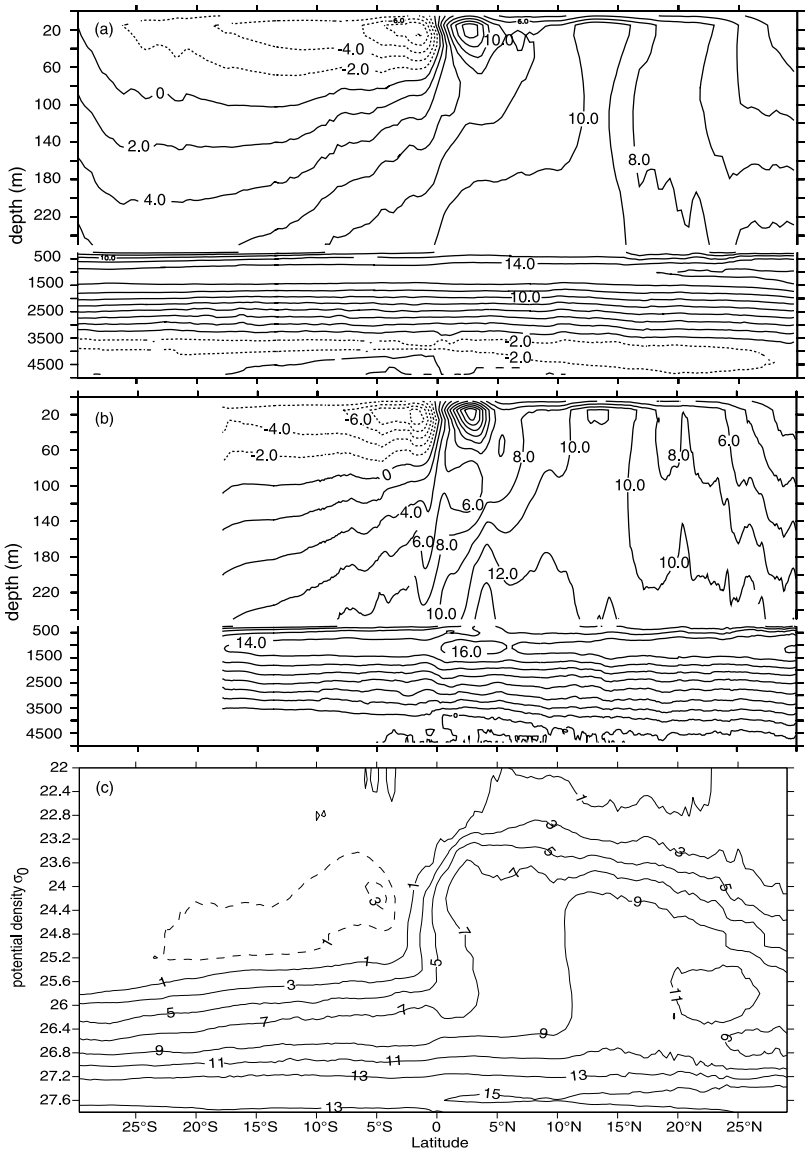

Figure 1. Meridional overturning stream function as a function of latitude and depth (m) for (a) Exp. 1 (mean 1958–1999), (b) Exp. 2 (mean 1987–1999) and as a function of potential density for (c) Exp. 1 (mean 1958–1999).

associated with recirculating water in the tropical cells (TCs [*Lu et al.*, 1998; *Molinari et al.*, 2004]). As shown in previous studies [*Hazeleger et al.*, 2003], the TCs are not associated with significant mean diapycnal transports and tend to disappear when considering eddy activity and integrating the flow in density instead of z-coordinates, thus eliminating isopycnic recirculation water [*Kröger*, 2001] (see Figure 1c).

[20] The Eulerian and Lagrangian depictions of the flow field in the thermocline layer (σ_θ = 24.4–26.2 kg/m^3) (Figure 2) confirm the interhemispheric asymmetry in the equatorward transports, and emphasize a predominant pathway along the western boundary in the source waters of the EUC. The models NBC (or NBUC, as it is referred to south of 5°S by some authors) is fed by a broad SEC pattern south of 6°S, with the bulk of the boundary flow being collected south of 10–11°S, in accordance with the observational picture obtained from multi-year transport measurements by *Schott et al.* [2005].

[21] The fate of water parcels crossing the equator in the NBC, i.e., their retroflection into the EUC and NECC, is heavily obscured in a long-term mean Eulerian field due to the strong intra-seasonal and seasonal variability in this regime (as discussed, e.g., in the FLAME model analyses of *Böning and Kröger* [2005] and *Stramma et al.* [2005b]). However, there are two clear pathways distinguishable: a continuous flow into the Carribean and a near-surface (σ_θ < 25.5 kg/m^3) fraction deflecting into the seasonal NECC and partly looping back towards the equator feeding the EUC.

[22] The sources of the EUC are delineated most clearly by a back-tracing of water parcels. We performed different backward integrations of the EUC water masses at 0°W. The integration was done using the mean annual cycle of Exp. 1, i.e., 12 monthly means that are repeated after one year

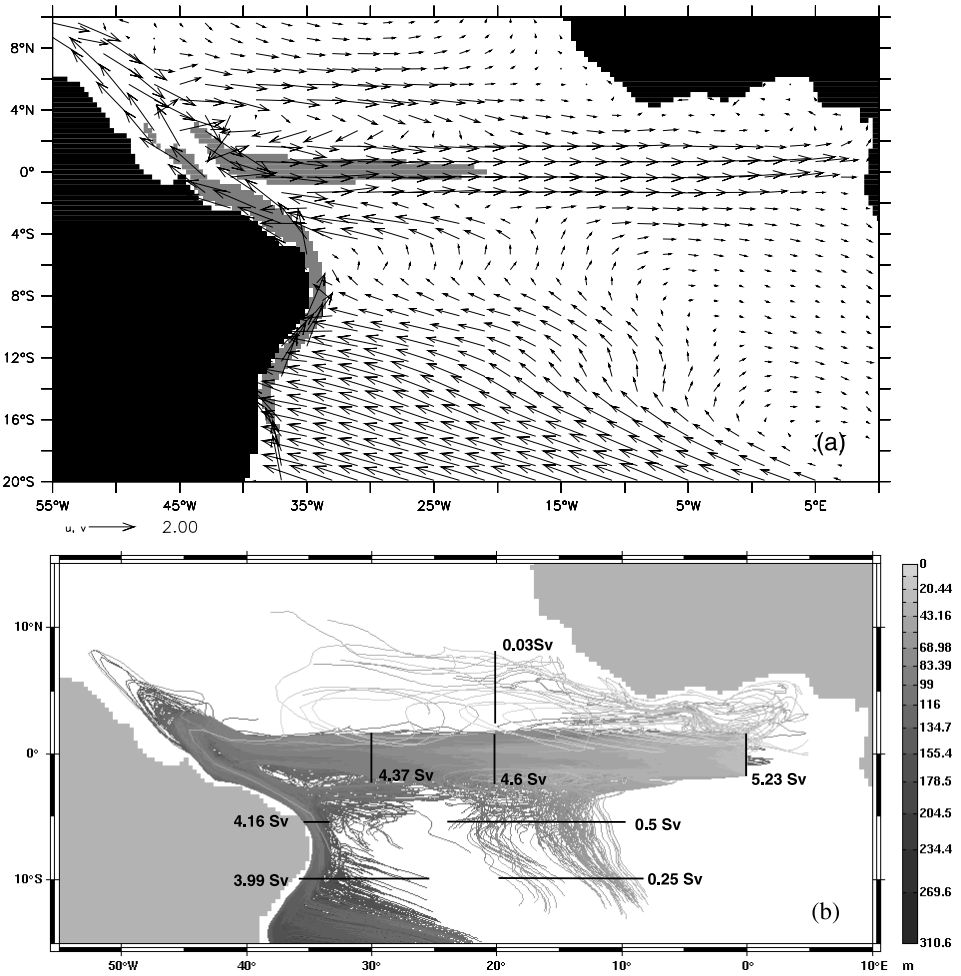

Figure 2. Different views of the mean circulation in Exp. 1: (a) Eulerian mean for the density range σ_θ = 24.4–26.2 kg/m^3 (shaded: velocities over 10 cm/s; note that for a better visualization of the interior flows the vector lengths are capped at velocities of 2 cm/s) and (b) floats launched in October in the EUC at 0°W and integrated backward in time for 4 years. Note the broad southern interior window visible and the strong inflow via the NBC into the EUC after a partial retroflection at about 4°N.

integration. We did the calculations starting at different seasons of the year and integrated backward in time for 4 years in each experiment. These realizations appear fairly robust in the main features: the bulk of the EUC is supplied by the NBC and some weak interior flow, whereas there is no clear connection to the northern hemisphere subduction region. However, the southern interior transport shows some seasonality with strongest supply from the interior pathway when floats at 0°W are inserted in February. Figure 2b examines the pathways of the various contributions to the EUC from the October run, where we have nearly maximum EUC transports at 0°W. The transport across this section, 5.23 Sv in the density range σ_θ = 24.4–26.2 kg/m^3 is fed almost exclusively by southern hemispheric thermocline waters: while the main path along the western boundary is clearly dominating, a small (5–10%) fraction is due to an interior window between 10°W and 20°W. This pathway is rather difficult to see in Figure 2a because velocities are very low (less then 1 cm/s) in this area. This interior window is not confined to a certain density or depth range and covers the whole thermocline. The transport values in Figure 2b resemble the transport through this section at the end of the integration, giving a good indication for the importance of the various EUC sources. (Note that the transports do not sum up to the launch transport of 5.23 Sv because some watermasses (re)circulate between the sections.)

[23] The Lagrangian analysis clearly emphasizes the negligible contribution of northern hemispheric source waters to the EUC, indicating an even more pronounced hemispheric asymmetry than previous model studies: while *Jochum and Malanotte-Rizzoli* [2001] and *Kröger* [2001] reveal some float trajectories following zigzag-pathways from the NEC, via the NECC and nSEC to the equator, the blocking of such communication by the potential vorticity ridge associated with the northward shift of the ITCZ in the equatorial Atlantic [*Malanotte-Rizzoli et al.*, 2000] appears very effective in the present model. We note that the for the main pathways and asymmetries of the EUC source waters, there is little difference between the 1/3°- and 1/12°-model versions; however, the latter, due to its much better resolution of the equatorial current regime (see Figure 3 below), shows

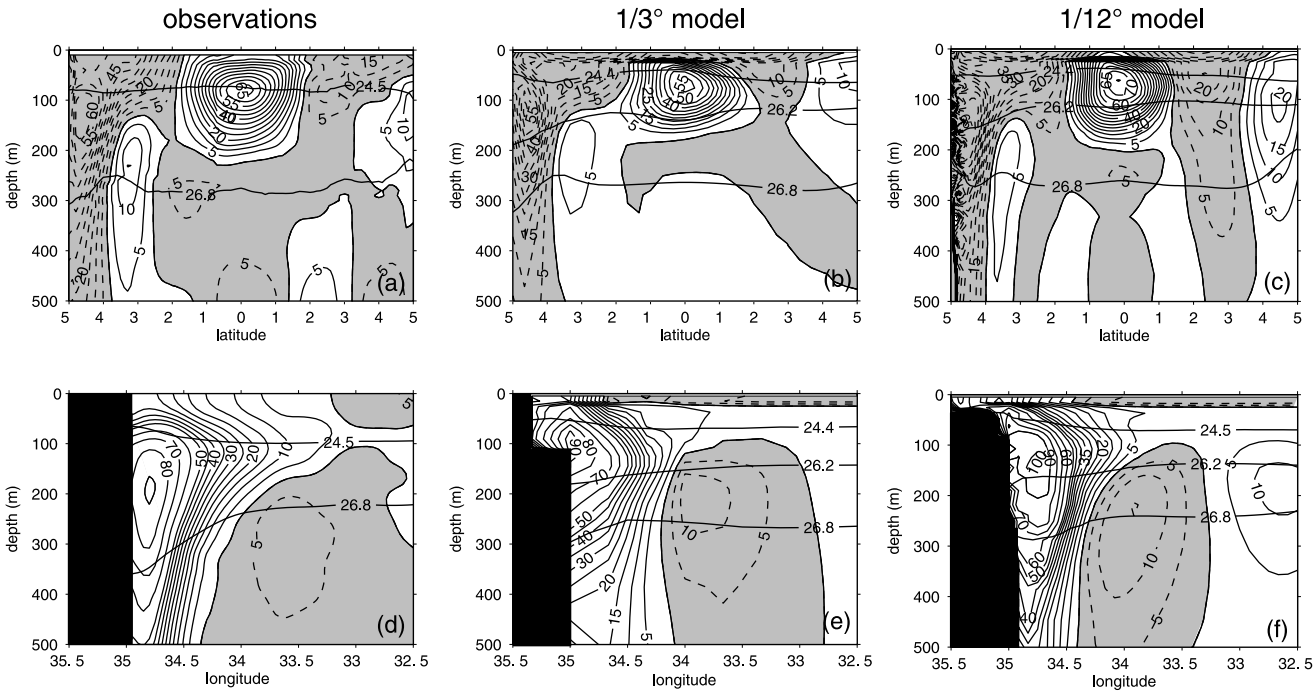

Figure 3. Current sections: (a) EUC at 35°W from 13 observations by *Schott et al.* [2003], (b) mean EUC (1958–1999) at 35°in the 1/3°-model (Exp. 1), (c) mean EUC (1987–1999) at 35°W in the 1/12°-model (Exp. 2), (d) NBC at 5°S from ADCP- and current meter observations by *Schott et al.* [2005], (e) mean NBC (1958–1999) at 5°S in Exp.1, and (f) mean NBC (1987–1999) at 5°S in Exp. 2.

much more detail in the zonal pathways, particularly a distinct presence of off-equatorial undercurrents (NEUC, SEUC); a discussion of the role of these features is, however, beyond the scope of the present paper. In summary the sources of the EUC in the present model are nearly completely located in the southern hemisphere.

[24] An assessment of the simulated mean current patterns and transports is provided for an EUC-section at 35°W and a NBC-section at 5°S (Figure 3), in comparison to the observational results presented by *Schott et al.* [2003, 2002]. While the 1/3°-model appears capable of representing the broader-scale aspects of the current system, the higher resolution is obviously needed for capturing the details of O(100 km) or less. The observed core speed of the EUC of more than 65 cm/s is well reproduced in the 1/12°-case. The maximum velocities are smaller (55 cm/s) in the 1/3°-case, along with a somewhat more diffuse meridional extent, both probably attributable to the use of a harmonic (Laplacian) mixing scheme for momentum in the model version considered here. *Böning and Kröger* [2005] and *Kröger* [2001] showed that using a biharmonic mixing scheme or higher resolution helps to sharpen the eastward equatorial undercurrents and to maintain the equatorial thermocline structure to a more realistic representation. So we could expect a much better representation of the EUC and the vertical density structure in the 1/12°-model. In both models, the EUC core lies between 50 m and 100 m and between the isopycnals $\sigma_\theta = 24.4–26.2$ kg/m^3, at slightly lower densities than in the observations. The mean transports in this density range are 8.5 Sv for the 1/3°- and 11.0 Sv for the 1/12°-case (total eastward transports are 16.1 Sv and 22.2 Sv, respectively), in comparison to the observational estimates of 12.3 Sv (for the layer σ_θ = 24.5 to 26.8 kg/m^3). The large differences between the two models results from the different vertical stratification (especially below $\sigma_\theta = 26.2$ kg/m^3) because the 1/3°-model is not able to maintain a very realistic thermocline structure for the reasons discussed above.

[25] The meridional velocity patterns at the western boundary (5°S) are all characterized by a strong (90–100 cm/s) NBC, with a subsurface current core. Thermocline-transports associated with the NBC between σ_θ = 24.5 to 26.8 kg/m^3 are 14.5 Sv for the 1/3°-model and 16 Sv for the 1/12°-version, somewhat stronger than the observational value of 13.4 ± 2.7 Sv estimated by *Schott et al.* [2002] from 6 repeated shipboard profiles. Moving to the density range given above, transports reduce to 9.3 Sv for the 1/3°-model and 8.7 Sv in the 1/12°-case. The somewhat different locations of the core relative to the topography, and the deeper core-depth in the observational picture, may partly be attributable to sampling issues (no data from the shelf, and a possible seasonal bias due to the lack of winter data), and the varying degree with which topographic details are represented at the different model resolutions.

[26] As a final check on the mean current distribution, a zonal section of the EUC at the equator for the 1/3°-case and 1/12°-case is provided in Figure 4. As discussed previously by *Oschlies and Garcon* [1999], the eastward penetration of the EUC is very sensitive to choices of the subgrid-scale mixing schemes, in particular the vertical viscosity. The present, simple realization of a stability dependent coefficient, produces a mean EUC extending across the basin, albeit with somewhat weak velocities in its eastern portion, particularly in the 1/3°-case. The iso-

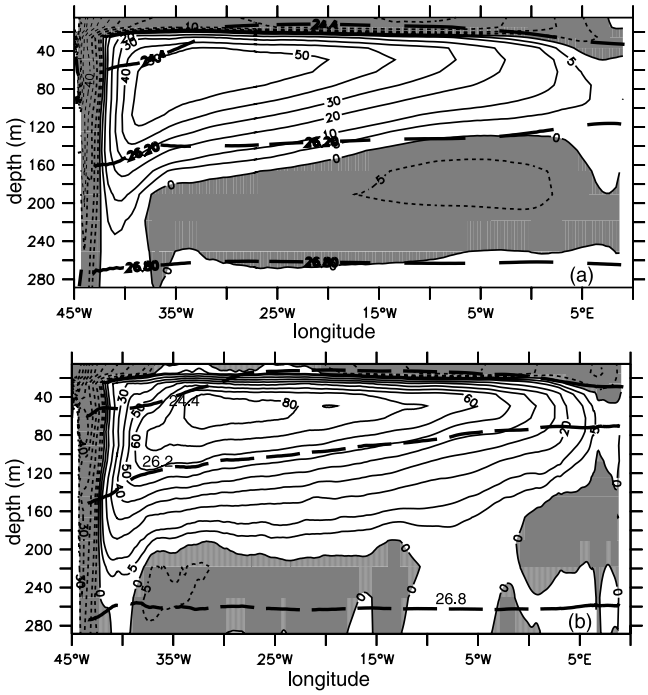

Figure 4. Zonal velocity and density section along the equator: (a) mean (1958–1999) from Exp. 1; (b) mean (1987–1999) from Exp. 2.

pycnals range of σ_θ = 24.4–26.2 kg/m^3 as discussed in Figure 1c for the 1/3°-model, appears representative for the EUC-layer for the central and eastern basin; we will thus use it for defining the vertical limits for the discussion of the transport variability in the following sections, instead of the somewhat denser isopycnal range suggested by *Schott et al.* [2003]. While the thermocline structure of the 1/12°-model looks quite realistic, the 1/3°-version shows too weak transport in the layers below σ_θ = 26.2 kg/m^3. We note that, compared to *Hazeleger et al.* [2003, Figure 1b], the EUC-core in the present models is found at shallower depths, and the vertical extent of the current is smaller. It is tempting to speculate that such model-model differences may lead to some quantitative differences in the weighting of the various source waters feeding the EUC: e.g., *Hazeleger et al.* [2003] show in their analysis a small but clear connection of the EUC to the northern subtropics that may be caused by a stronger transport below 100 m and a corresponding weaker transport in the near surface layers from the southern hemisphere (however, the total EUC transports of both models do not differ very much). These conditions may cause a stronger northern inflow in their model into the upper part of the EUC.

[27] Another factor determining the slightly different supply of both fractions compared to the present solution could, however, be the relatively weak MOC transport in the OCCAM model which is potentially more favorable for northern pathways to the equator: the northern supply in their study is 1.25 Sv (0.85 Sv from western boundary, 0.4 via the interior pathway), but the main part (8.51 Sv) of EUC water comes from the south: 7.88 Sv by western boundary exchange and 0.71 Sv by interior transport, i.e., a transport ratio north/south of 1/7. From our lagrangian analysis we get only a weak seasonally varying northern inflow of 0.03 Sv from the interior.

3.2. Annual Cycle

[28] The basic physical mechanisms of the wind-driven annual cycle were elucidated by *Philander and Pacanowski* [1986]. They illustrated a direct link between thermocline depth, EUC transport and zonal wind stress but also showed the importance of Rossby waves for the annual cycle. Various model studies have dealt with their generation and propagation characteristics [e.g., *Thierry et al.*, 2004] and have examined their signatures in the deep [e.g., *Böning and Kröger*, 2005] and intermediate [*Brandt and Eden*, 2005] layers of the equatorial Atlantic. An expression of the wave signal in the near-surface currents along the equator is given in Figure 5, showing the anomalies of the zonal velocity component from the annual-mean, at 100 m depth in the 1/3°-model. The wave signal extends nearly across the whole basin, characterized by an amplitude of O(10 cm/s), intensified to O(15–20 cm/s) between 20°W to 35°W, and decreasing to the western boundary. The phase propagation from 10 W to 35 W takes about 2 to 4 months.

[29] In the 1/12°-model the wave behavior is less clear above about 500 m because of a much stronger intraseasonal variability due to, e.g., tropical instability waves. The analysis of these waves and their role in the mean current structure and the annual cycle is beyond the scope of this paper.

[30] As already shown for the mean transport of both models there is a notable difference in the vertical extent of the EUC, resulting in quite different behaviors concerning the annual cycle at 35°W (Figure 6): while the 1/3°-case shows a clear annual harmonic, the 1/12°-case reveals two distinct maxima throughout the year. Comparable in phase is only the September-maximum, whereas the second maximum in early spring is missing in the 1/3°-version. A possible reason for the similarity in the autumn maximum is that this feature is primarily caused by wind-forcing, which is the same in both models. In the winter season the EUC in the 1/3°-model seems to be underestimated because the thermocline part is unrealistically weak in this version. *Hazeleger et al.* [2003] also find a two-maxima annual cycle in their analysis of the OCCAM 1/4°-model. In their case both peaks were of comparable strength, in our case the March-maximum dominates. The phases of both solutions are comparable.

[31] Obviously, the strong variations on seasonal to intraseasonal timescales render a quantitative assessment of the simulated mean annual cycles by observational estimates obtained by *Schott et al.* [2003] very difficult, as indicated by the scatter (Figure 6) in the values.

[32] The annual cycle of the NBC transport at 5°S (Figure 6) also shows a strong dependence on resolution: while the 1/3°-model shows a clear annual signal with maximum in June and minimum in December/January, the 1/12°-case suggests three maxima: in March, June and October.

[33] It should be noted that the characteristics of the seasonal variations of the EUC and NBC do not correspond to each other: while the mean flows are clearly connected, with the EUC primarily supplied through the NBUC/NBC route (Figure 2), this does not hold for the variability: while the seasonal cycle at 5°S is fairly representative for the west-

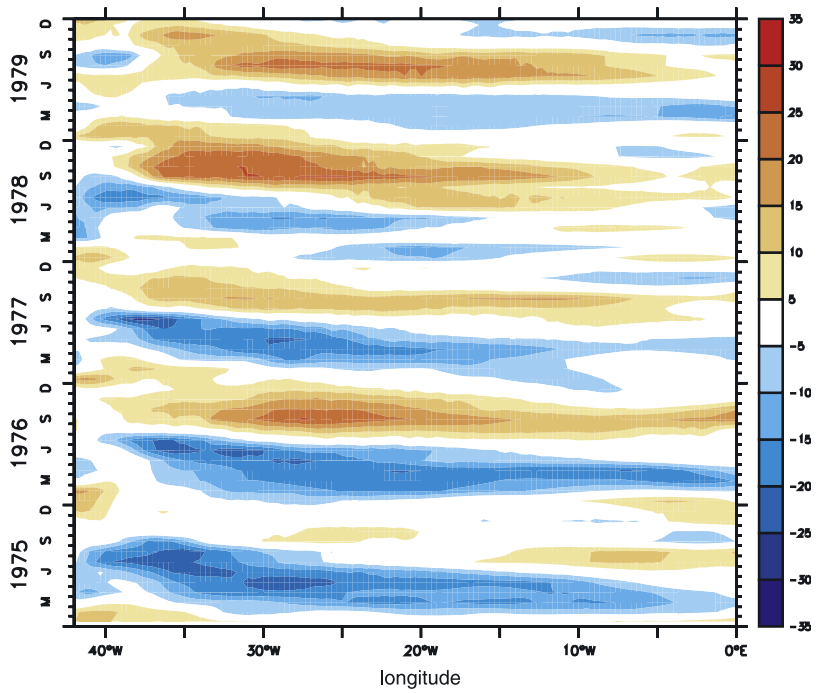

Figure 5. Hovmoeller diagram of zonal velocity anomaly at the equator in 100m depth from Exp. 1, indicating a Rossby-wave signal with interannual modulation.

ern boundary regime as far south as 10°S, the EUC appears strongly influenced by the local forcing close to the equator, a difference that will be seen again in the characteristics of the interannual variability, discussed in the next section.

4. Interannual to Decadal Variability

[34] It appears useful to begin the investigation of the low-frequency variability by first examining the characteristics of the transport time series. Figure 7 depicts recordings of the EUC transport (at 35°W, left panel) and of the NBC (at 5°S, right panel), for different model cases (Exps. 1, 2 and 3), and different choices of cross sections. The unfiltered series of monthly mean values in the experiments 1 and 2 (Figures 7a and 7b) appears dominated by the seasonal cycle and intraseasonal fluctuations (see also Figure 6), clearly modulated by a year-to-year and longer-term variability. It is remarkable that the high frequency

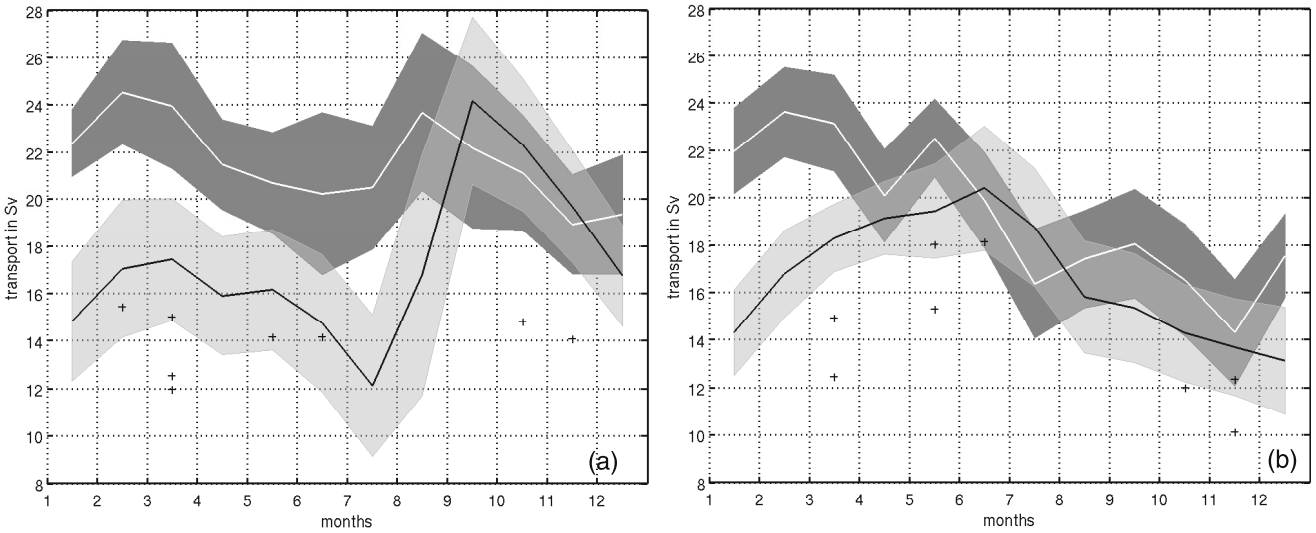

Figure 6. Mean annual cycle of (a) EUC volume transport (in Sv) at 35°W and (b) NBC volume transport (in Sv) at 5°S. Black line: Exp.1, white: Exp. 2. The shaded areas give the standard deviation of monthly values over the model periods. The marks are observational transports calculated from the measurements done by Schott et al. [2003, 2005] for the depth range 50–300 m.

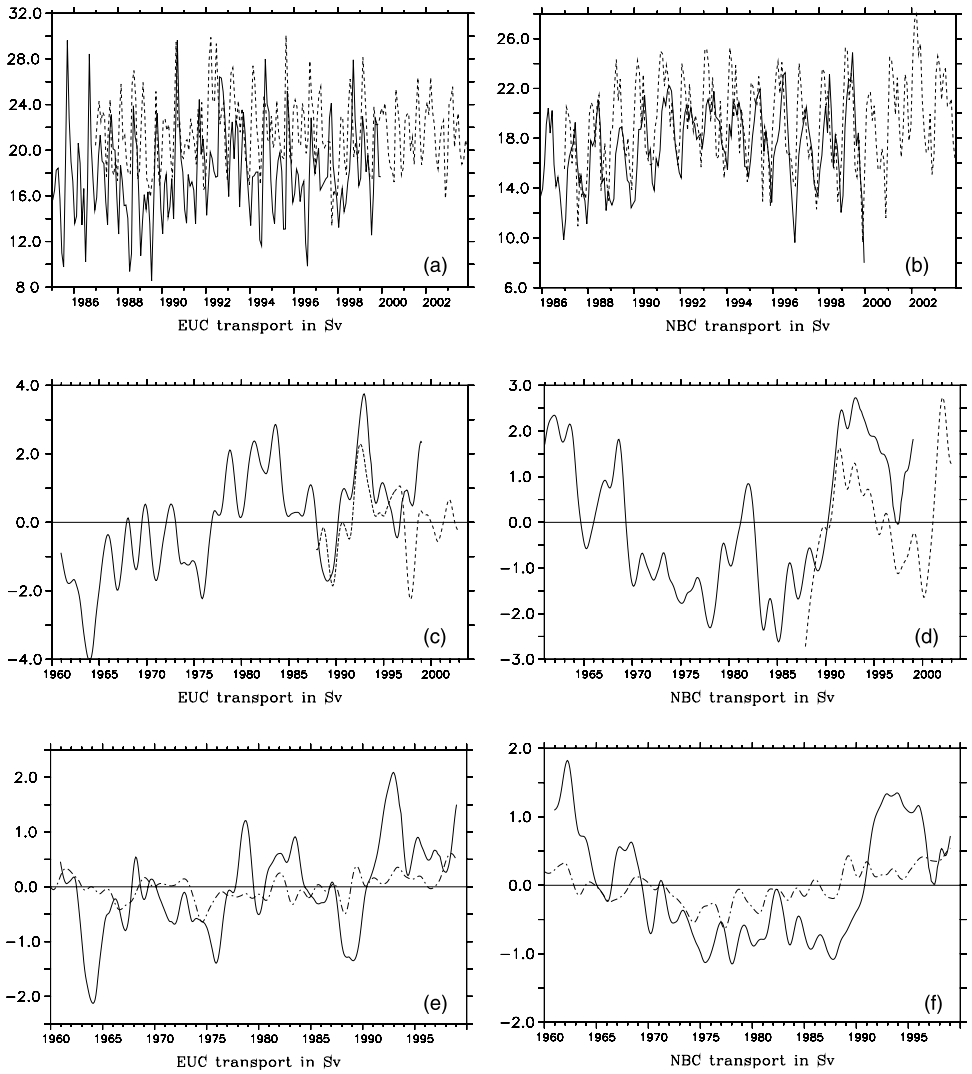

Figure 7. Time series of volume transports (in Sv): (a) EUC transport at 35°W in Exp. 1 (full) and Exp. 2 (dashed), (b) NBC at 5°S in Exp. 1 (full) and Exp. 2 (dashed), (c) 2-year filtered anomaly time series of EUC transport at 35°W in Exp. 1 (full) and Exp. 2 (dashed), (d) 2-year filtered anomaly time series of NBC transport at 5°S in Exp. 1 (full) and Exp. 2 (dashed), (e) 2-year filtered anomaly series of EUC transport at 35°W in Exp. 1 (full) and Exp. 3 (dash-point) in the density range $\sigma_\theta = 24.4-26.2$ kg/m^3, and (f) 2-year filtered series of NBC transport at 5°S for Exp. 1 (full) and Exp. 3 (dash-point) for the same density range as in Figure 7e.

variability is more pronounced at the 35°W EUC section where it seems to reduce the annual cycle of Exp. 2 relative to Exp. 1, whereas the NBC at 5°S shows an enhancing of the annual cycle (compare also Figure 6). The low-frequency signal is highlighted (Figures 7c and 7d) by a 2-year low-pass filtered series of the respective transport anomalies (deviations from the mean transports of the models integration period). Considering the eastward (for the EUC) and northward (NBC) velocity components both currents reveal a significant (inter-)decadal variation, with rather different characteristics: while the EUC exhibits an increase from a minimum in the early 1960s to positive anomalies during the late 70s to early 80s, and a distinct maximum in 1993, the NBC is marked by a gradual weakening from the early 60s to mid-80s, and a pronounced recovery thereafter. It is remarkable to find only rather weak differences (a small shift of the anomaly signal due to the different mean states of Exp. 1 and Exp. 2) in the simulated decadal variation over the 1990s between Exp. 1 and Exp. 2 for the NBC (Figure 7d), indicating a much weaker sensitivity to model resolution for these timescales as compared to the (intra-)seasonal variability. However, the EUC variability (Figure 7c) in both experiments differs due to the much stronger high-frequency variability resolved by the higher resolution in Exp. 2. Further analysis of the low-frequency variability will henceforth mainly build on the longer 1/3-integrations.

[35] A first indication to the mechanisms of the transport changes is provided by a comparison of the 1/3-reference case (Exp. 1) using interannually varying fields for both wind stresses and heat fluxes, with Exp. 3 where wind

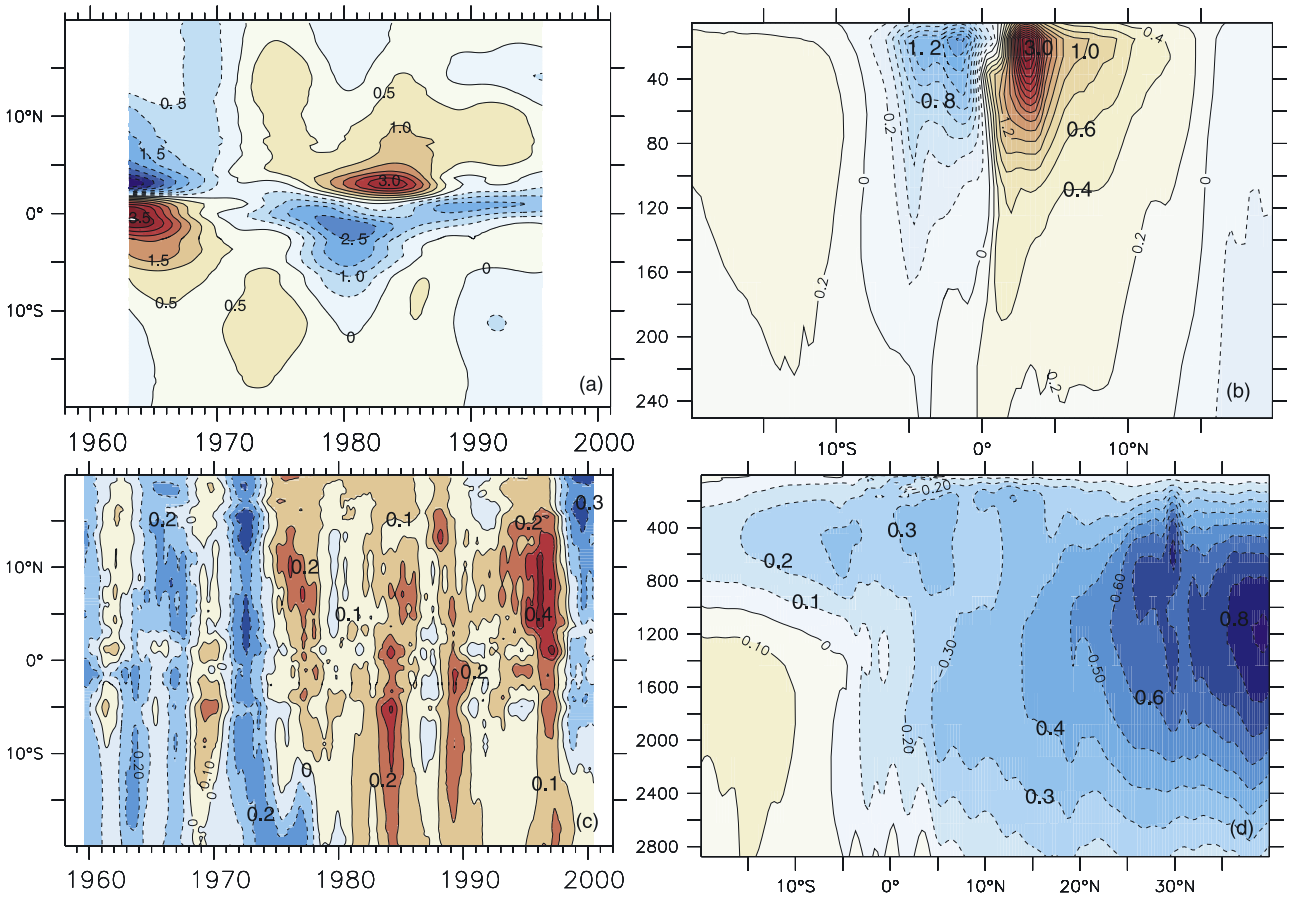

Figure 8. Zonally integrated meridional transport anomalies (in Sv): (a) Hovmoeller diagram of 5-year low-pass filtered transport anomalies in the upper thermocline (80m) from Exp. 1, (b) vertical structure of the 1980–1985 anomaly in Exp. 1, (c) Hovmoeller diagram of 3-year low-pass filtered transport anomalies in the thermocline (300m) from Exp. 3, and (d) vertical structure of the 1972 anomaly in Exp. 3.

stresses were replaced by climatological, monthly mean fields (Figures 7e and 7f). In contrast to Figures 7a–7d we now integrate the transports over the density range σ_θ = 24.4-26.2 kg/m^3, allowing some inferences about associated heat transport anomalies of the decadal signal.

[36] Obviously, the bulk of the transport variability is tied to the variation in the wind stresses, corroborating previous model results [e.g., *Kröger et al.*, 2005]. In comparison to Figures 7c and 7d the decadal signal exhibits a similar phase, but a reduced amplitude, primarily due to the smaller vertical range of the integration. A decadal signal is also visible in the NBC time series of Exp. 3 (Figure 7f) with even more reduced amplitude. The origin of the decadal signal will be elucidated further by considering the variability characteristics observed at these particular sites in the context of the basin-scale transport patterns.

4.1. Subtropical-Tropical Transport Patterns

[37] A view of the decadal variability in the strength of the shallow subtropical-tropical overturning cells is provided in Figure 8a, by depicting the anomalies (from the long-term mean) of the zonally integrated meridional transports as a function of latitude and year, analogous to *Kröger et al.* [2005, Figure 3]. The Hovmoeller diagram for Exp. 1 reveals patterns very similar to their reference case: a variability of comparable amplitude in the southern and northern hemisphere, despite the strong asymmetry in the mean STC strengths; amplitudes are highest close to the equator, indicative of a pronounced variability of the TCs. (Note that positive (negative) anomalies in the northern (southern) hemisphere correspond to enhanced cell strengths, i.e., enhanced equatorward transports of thermocline water.) Weaker than average cell strengths in the late 60s are followed by a prolonged period of enhanced transports, with maxima (slightly out of phase between the north and south) from the late 70s to mid 80s. The vertical structure of this variability signal is exemplified for the period of enhanced cell transports during 1979–1986. Figure 8b reveals a similar pattern of strengthened STC/TC-cells over this period in both hemispheres, with equatorward transport anomalies mostly confined to the upper 100 m in the density range σ_θ = 24.4–26.2 kg/m^3 for the southern and σ_θ = 23.5–26.2 kg/m^3 for the northern hemisphere.

[38] The close correspondence between the solutions of two different models (primitive equation in this study versus reduced gravity in the case of *Kröger et al.* [2005]), different basin configurations (Atlantic basin versus subtropical-tropical domain), and different atmospheric forcing concepts (linearized bulk formula versus atmospheric mixed layer model) corroborates previous conclusions of a dom-

inance of a local wind stress-related generation mechanism, and emphasizes the overriding importance of the choice of the wind product (which in both model cases is based on the same reanalysis fields) in the simulation of this variability.

[39] The behavior of the reference case is contrasted in Figures 8c and 8d with the solution of Exp. 3, illuminating the comparatively small contribution of transport anomalies associated with the variable thermal forcing. There are two main differences in the zonally integrated transport patterns compared to the wind stress-related anomalies. First the transport changes are of a much broader latitudinal and vertical extent, i.e., the anomaly patterns are not confined to the surface of the equatorial regime, but appear to be a part of a basin-scale pattern that involves changes in the deep MOC (Figure 8d). Second the meridional transport changes in the tropical thermocline tend to be of the same sign in both hemispheres, corresponding to a dipole-like waxing and waning of the northern and southern STC cells (Figures 8c and 8d). The decadal variation is characterized by weaker than average northward transports in the tropical thermocline (corresponding to a weaker southern STC) until the mid-1970s, with a distinct minimum around 1973, replaced by some 20 years of enhanced transports, with maxima during the mid-80s and (in the northern hemisphere) early 90s, and a subsequent steep decline from 1997 to 1999. (Note that we have chosen to apply a more narrow 3-year low-pass filter in Figure 8c, in order to retain some fraction of the signal in the late 90s.) The spatial and temporal characteristics of the heat flux-related variability in the tropical transports are first indications of an association of this signal with the deep meridional overturning circulation. As will be corroborated below by the dedicated response experiment (Exp. 4), the meridional transport changes in the tropical thermocline can be interpreted in terms of a remote forcing mechanism. The changes in the deep meridional overturning circulation can be related to the variability of deep water formation in the subpolar North Atlantic and will be discussed in section 4.3.

4.2. Manifestation of Transport Anomalies in Equatorial Currents

[40] Before turning back to the mechanism of the remotely driven contribution to the tropical transport variability in the subsequent section, we will examine what spatial current patterns correspond to the zonally integrated transport anomalies. The standard deviation of the interannual meridional transport anomaly in the tropical thermocline, taken as the range of $\sigma_\theta = 24.4–26.2$ kg/m^3 for the whole integration period (1958–1999) of Exp. 1 (Figure 9a), reveals a band of maximum variability along the western boundary, suggesting a strong contribution of the NBC to the zonally integrated transport changes, and a possible potential of the NBC transport as an index for the strength of the southern STC. Closer inspection, however, reveals important modifications of this view: Figure 9b provides an illustration of the upper-thermocline (50–100 m) flow anomalies relating to the phase of intensified STC-cells during 1980–1985 (compare Figure 8b for the vertical structure). The enhanced northern transport in the southern STC-cell appears clearly associated with stronger northwestward SEC flows in a broad regime south of the equator, and an increased EUC along the equator. However, in a remarkable deviation from the annual-mean pattern, the increased SEC flow towards the western boundary does not lead to a northward, but a southward transport anomaly along the NBC, most clearly in the latitude range 4°S to 12°S. The current anomalies in the northern hemisphere show a more complicated pattern near the western boundary, reflecting the fact that changes in the NBC associated with the southern STC are also manifested north of equator, in the retroflection regimes and source areas of the EUC and NECC. The identification of a current signature associated with the northern STC variability remains ambiguous although the anomaly patterns hint at a variation of northern supply of the EUC through zig-zag pathways from NEC via the NECC and northern SEC.

[41] The question of the relation of the NBC transport variability to the zonally integrated STC transport is examined further in Figure 10, where it appears instructive to contrast the wind stress-related variability governing the reference case (Exp. 1), with the MOC-related contribution brought out by Exp. 3. In Figure 10a the contribution to the net equatorward transport anomalies is examined by accumulating the meridional transports along 5°S from the eastern boundary for the period 1980–1985 for which both experiments show enhanced northward transport in the zonal integrated patterns. In Exp. 1 the northward transport anomaly is due to enhanced SEC transports over a broad interior region, which are partly compensated by a southward transport anomaly in the NBC at the western boundary. The compensating tendencies of the STC transport anomalies in the interior (between 10°E to 33°W) and the western boundary current (33°W to 36°W) appear analogous to the behavior observed in the Pacific at interannual and decadal timescales for the period 1980–2000 [*Lee and Fukumori*, 2003] as well as for the longer period 1958–1997, which includes the 1976–77 climate shift [*Capotondi et al.*, 2005]. Exp. 3 shows a rather different manifestation along this section: a weakened SEC between 33°W and 5°E and a strong northward anomaly in the NBC between 33°W and the western boundary. However the amplitude of this signal is much smaller than the wind-induced one and therefore hidden in the reference case.

[42] The contrasting zonal distributions of the wind-driven and MOC-related signals are reflected clearly in a comparison of time series of the NBC-transport with the zonally integrated flow. The difference between curves reflects the variations of the interior flow. Figure 10b shows time series of both variables at 5°S for Exp. 1 and Figure 10c for Exp. 3. The opposite tendency of the NBC in relation to the net meridional flow is obvious for Exp. 1 in nearly all years, while a close relationship between NBC and net transport exists if the variable wind forcing is switched off (Exp. 3). This link is fairly representative for a wide latitudinal range as indicated by the correlation of NBC strength and zonally integrated transport (Figure 10d). For Exp. 3 the correlation coefficient is high and nearly independent of latitude (0.7–0.8) while Exp. 1 shows no clear connection between both variables south of 8°S and an increasingly positive correlation from about 5°S to the equator. This behavior is already suggested by Figure 2a: zonally integrated transports and the NBC north of 4°S only correspond to each other in this region because the SEC bifurcates between 4°S and 8°S. In Exp. 3 the bifurcation

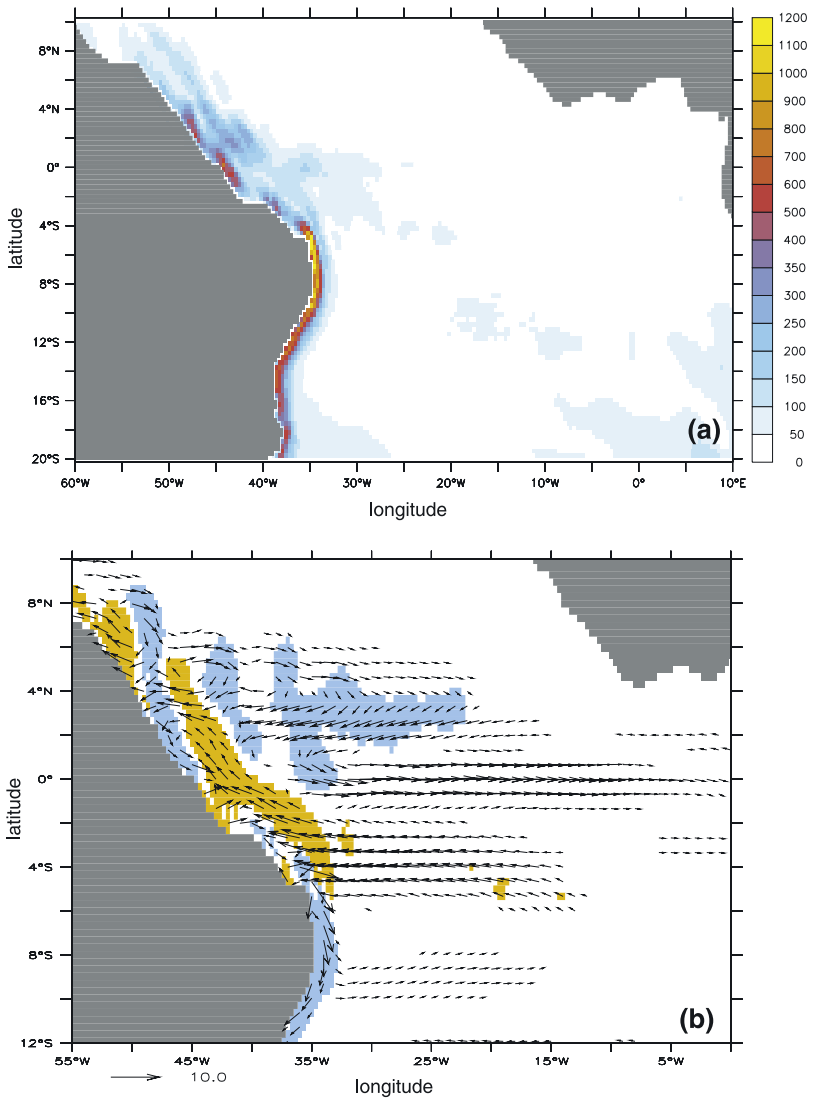

Figure 9. Spatial patterns of variability corresponding to anomalies in the meridional transport in Exp.1: (a) RMS changes in meridional transport per unit longitude for the layer σ_θ = 24.4–26.2 kg/m^3; (b) horizontal velocity anomalies in 50–100 m for a period of enhanced equatorward transports (1980–1985); yellow: areas of positive northward flow anomalies >5 cm/s, blue: areas of negative anomalies <5 cm/s.

latitude does not vary, so there is no variability of the interior flow that leads to changes in the NBC. From Figure 10b we would expect an anticorrelation of the NBC transport and the zonally integrated transport south of 5°S. Figure 10d shows only a very weak negative correlation which increases on longer timescales (maximum for 5-year-filtered time series) due to the adjustment of the Sverdrup circulation.

[43] The different behavior of NBC variability and the integrated transport bears consequences for the relation between NBC and EUC variability. As Figures 8b and 8d suggested the upwelling at the equator is connected to the equatorward transport in the thermocline. So we would expect a coherent behavior between the EUC and the NBC variability. Anyway, this connection could be complex, because on interannual timescales the wind-driven variability associated with a stronger SEC weakens the supply of NBC to the EUC, but strengthens the input from the ocean interior as shown in Figures 9 and 10.

[44] Figure 11 gives Hovmoeller diagrams of the NBC (as a function of latitude) and EUC (as a function of longitude) for Exp. 1 (Figure 11a) and Exp. 3. (Figure 11b) for the range σ_θ = 24.4–26.2 kg/m^3. Both experiments reveal the decadal signal in the NBC as described in Figures 7 and 8. As already indicated in our discussion of Figures 2 and 10, there is no evidence for a link between the EUC and the NBC variability for any latitude. Most NBC anomalies fade away or even reverse in the area between 4°S and the equator. The EUC variability appears hence unrelated to the behavior of the NBC farther south, partly due to the inflow of the SEC between 6°S and 2°S as indicated in Figure 9b.

[45] In contrast, Exp. 3 shows a relation between the EUC fluctuations in the western equatorial Atlantic and the NBC fluctuations further south, although not coherent through the

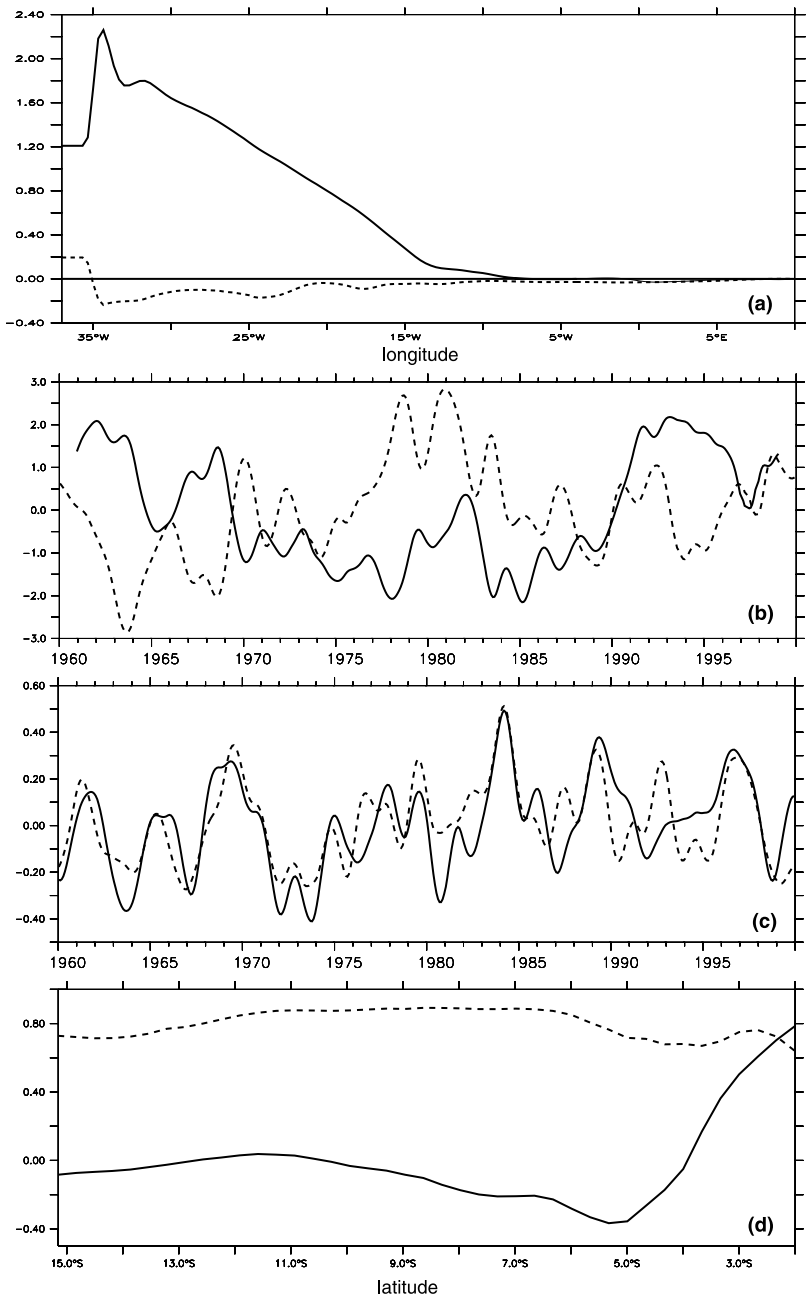

Figure 10. Relation between the NBC and the zonally integrated (STC) transports (in Sv) at 5°S: (a) cumulative transport anomalies for Exp. 1 (full) and Exp. 3 (dashed) from a five year mean for the period of enhanced zonally integrated northward transport (1980–1985); (b) time series of NBC (full) and integrated meridional transport (dashed) anomalies at 5°S for Exp. 1 (Figure 10b) and Exp. 3 (Fig ures 10c and 10d) correlation between NBC and STC transports as function of latitude for (b) (full) and (c) (dashed).

zonal extent of the EUC: the amplitudes decrease to the east, vanish at about 20°W and partly reverse east of 10°W. This behavior implies that decadal thermohaline signals are not manifested in the EUC, upwelling and SST variability in equatorial regions east of about 20°W. However, the variability signal in the NBC is associated with a cross-equatorial pattern as indicated by Figure 8c. The structure and mechanism of this variability will be discussed in more detail in the next section.

4.3. Remote Effects of Thermohaline-Driven Changes in the Subpolar North Atlantic

[46] The role of variations in the deep MOC associated with the variability in LSW formation is elucidated by an additional experiment (Exp. 4) which focuses on the system's response to a step-function shut-down of deep water formation in the Labrador Sea. Following the same spin-up as in Exp. 1, a permanent anomaly in the heat fluxes over the Labrador Sea was added to the climatological forcing in such a way that surface cooling in subsequent winters was

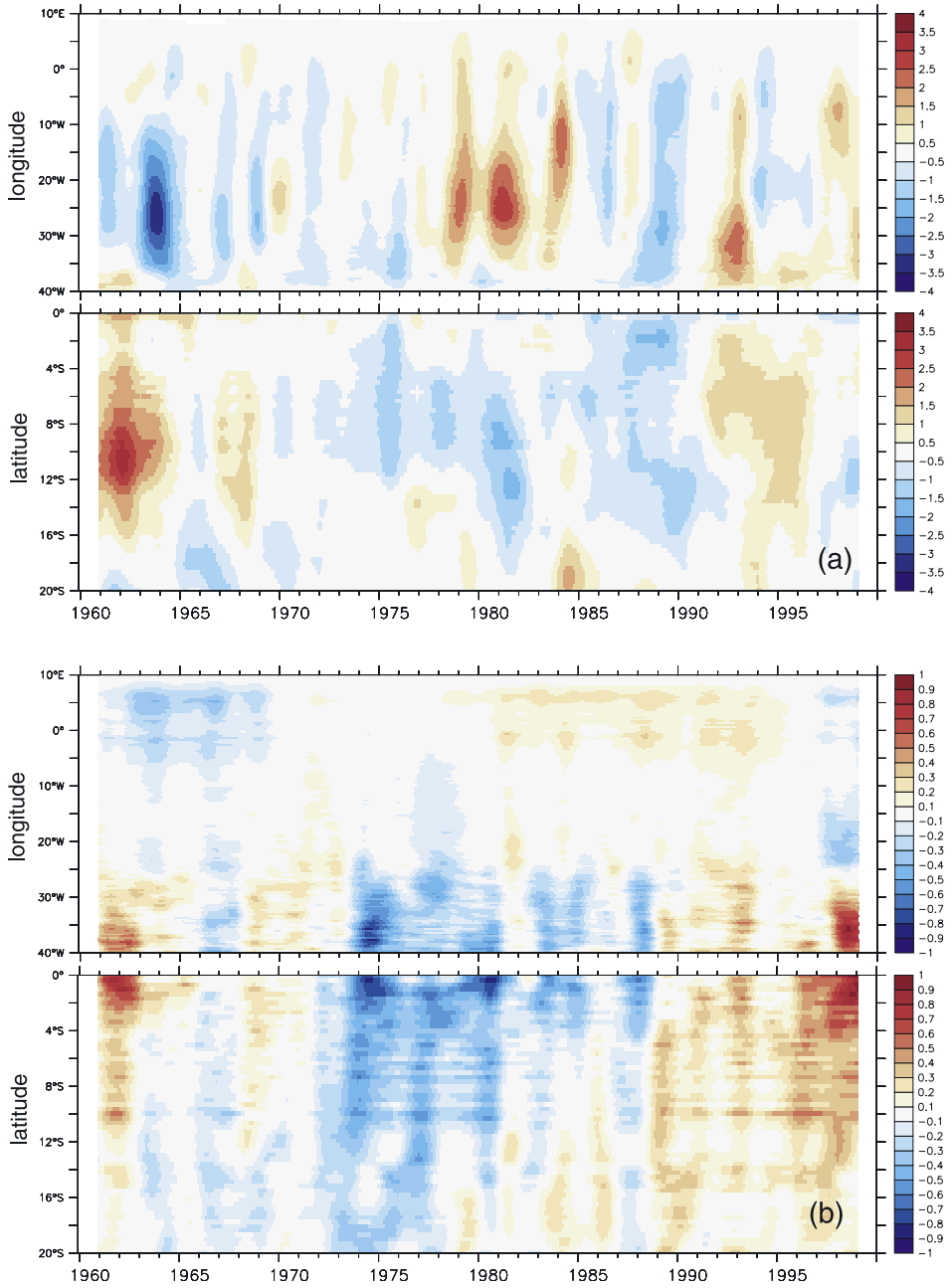

Figure 11. Relation between NBC and EUC variability: transport anomalies in Sv along the western boundary (averaged between 45°W to 30°W) and eastward transport anomalies along the equator for Exp. 1 (a) and (b) for Exp. 3.

capped at temperatures of 5°C, thereby effectively eliminating the deep winter convection and renewal of LSW. Note that this forcing anomaly does not affect the water mass transformations in the north-eastern North Atlantic, a setup differing from more idealized configurations as used, e.g., by *Yang* [1999]. In particular, the formation of the denser components of the NADW associated with the overflows from the Nordic Seas and their contributions to the MOC is basically retained, i.e., there is no interannual variability due to the restoring to climatological conditions in the region north of the overflows. Experiment 4 thus examines the effect of changes in the LSW formation in isolation, allowing a quantitative determination of an upper bound for the effect of LSW changes on the meridional overturning. The interpretation of Exp. 4 will be aided by a similar response experiment, based on the same 1/3°-Atlantic model, that has been used for the analysis of equatorward signal propagation of subpolar MOC anomalies by *Getzlaff et al.* [2005]: their case (denoted RESP 1/3) dealt with the response to a permanent heat flux anomaly corresponding to a NAO-index of 3, i.e., an enhanced LSW formation due to stronger winter heat losses; in addition, their case represented an ensemble of three experiments (differing in initial conditions), allowing to separate effects of internal fluctuations from the LSW-forcing related changes.

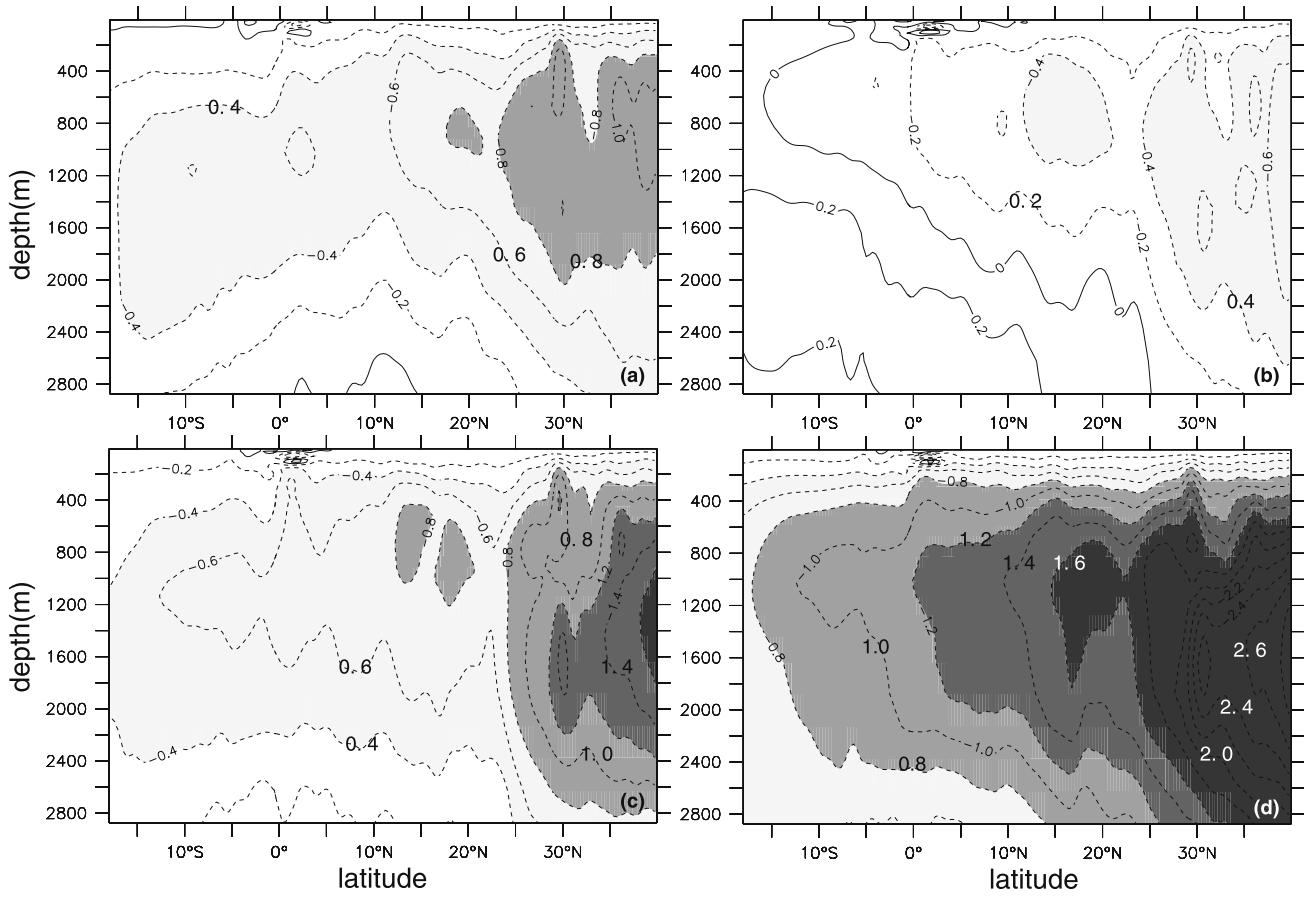

Figure 12. Reaction of the MOC in the tropical Atlantic to a cessation of Labrador Sea Water formation as simulated in Exp. 4 after: (a) 3 years, (b) 5 years, (c) 9 years, and (d) 15 years. Negative values indicate a weakening of the deep southward transport of NADW and a concomitant weakening of the zonally integrated northward transport in the upper 1000 m.

[47] The adjustment to a new equilibrium state after a perturbation of the basin-scale circulation and the role of oceanic waves in this process have been investigated both in idealized models [*Kawase*, 1987; *Johnson and Marshall*, 2002] and in models with realistic geometry [*Döscher et al.*, 1994; *Capotondi*, 2000]. We will focus our discussion to the effect of the adjustment process on the decadal variability in the equatorial current regime, i.e., we are not concerned here with the process of wave propagation itself. The temporal characteristics and spatial patterns of the zonally integrated transports (in the following named MOC) in the tropical Atlantic are provided in Figures 12 and 13. In both figures we show the resulting anomalies of the zonally integrated transports relative to the climatological initial conditions from Exp. 4: Figure 12 shows the anomaly signals in the meridional-vertical plane and Figure 13 gives the anomaly signal at 1000 m depth as a function of time.

[48] Figure 13 indicates a very fast response to the step-function change in the subpolar buoyancy forcing: after 2–3 years the anomaly signal has reached 40°N (a result also found in previous studies, e.g., by *Eden and Willebrand* [2001]) and is after that communicated more rapidly towards the tropics by coastally trapped waves [see, e.g., *Getzlaff et al.*, 2005, Figure 3]. In the fourth year after the cessation of convection, a peak signal of 1 Sv reduction of the southward transport arrives and crosses the equator at depth. The corresponding MOC transport anomalies in the meridional-vertical plane (Figure 12a) reveal a basin-scale pattern, with a reduction of cross-equatorial transports of about half the reduction in the meridional transports at 40°N. This initial, fast pulse in the MOC gives way to a relaxation phase

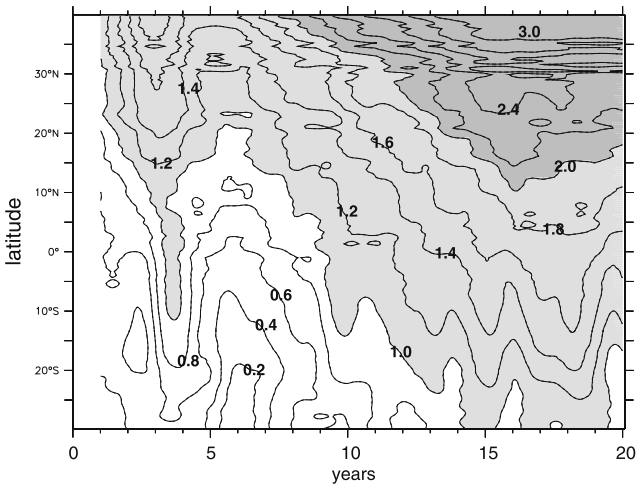

Figure 13. Meridional propagation of the MOC signal in 1000m following a cessation of LSW formation (Exp. 4).

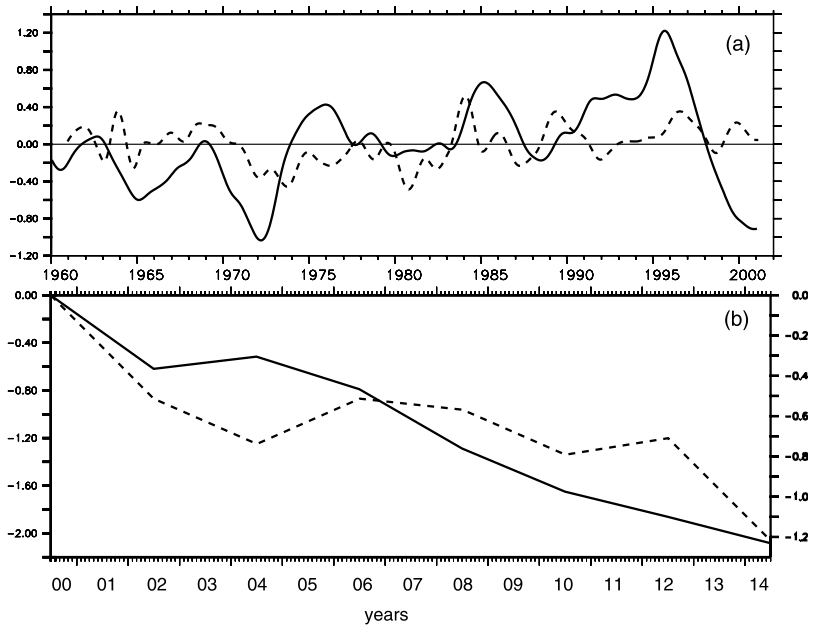

Figure 14. Anomalies of MOC transport (in Sv) at 45°N (full) in 1000 m depth and NBC transports (20–300 m) at 5°S (dashed): (a) for Exp. 3; (b) for Exp. 4. The scale on the right belongs to the transport at 5°S.

in the tropics, with a drop in the transport anomalies most strongly in the southern hemisphere (Figure 12b), followed by a more gradual increase on a decadal timescale (Figures 12c and 12d). Comparison with the complementary experiments (RESP 1/3) of *Getzlaff et al.* [2005] indicates a rather robust temporal behavior in the main characteristics of the tropical MOC response, i.e., an initial peak after 3–4 years followed by a O(5 year)-relaxation phase. Note, however, that their individual realizations demonstrate that the details of transport time series are affected by the superimposed internal variability. This also includes the phase of the signal: an initial, significant change in transport may already be felt in the tropics after 2 or only after 5 years.

[49] The MOC anomaly patterns in Figure 12 characterizing this idealized response experiment corroborate the hypothesis about the origin of the transport anomalies found in Exp. 3 (compare Figure 8d): the (inter-)decadal modulation of the equatorial transports can be understood as a manifestation of the dynamic response of the Atlantic's MOC to buoyancy-driven changes in the subarctic deep water formation.

[50] The relation between mid-latitude deep MOC changes and meridional transports in the equatorial Atlantic is examined further in Figure 14, for both Exps. 3 and 4 . Since the MOC anomaly patterns in the tropical Atlantic appear associated with changes in northward transport in the upper 1000 m (Figures 8d and 12) which are primarily manifested in the NBC along the western boundary (Figure 11), it is instructive to confront the time series of the MOC at 43°N with the NBC transports at 5°S. In Exp. 3 (Figure 14a) weaker northward transports at 5°S in mid-70s follow a low LSW phase at the beginning of the 70s and the strengthening of the NBC transports through the 80s to the mid-90s follows the trend in deep MOC. Because of the oscillating nature of the MOC response there is no clearly defined time-lag between the mid-latitude MOC and the NBC transport. Apparent lags for Exp. 1 (Figure 14a) between deep MOC and NBC variability lie in the range of 2 (1995–1996) to 5 years (1985–1989), probably reflecting the stochastic element in the transport time series due to the internal variability included in this eddying ocean circulation model. The response experiment (Exp. 4, Figure 14b) shows that the NBC transport basically follows the MOC trend, albeit with a much smaller amplitude and the relaxation behavior shown in Figure 12. The oscillatory behavior after the first response in year 4 is obvious. Together with the finding that thermohaline variability is confined to the western boundary current (see Figure 10c) we conclude that variability in the LSW formation primarily leads to a decadal modulation of the NBC variability.

5. Summary and Conclusions

[51] A sequence of experiments based on the FLAME hierarchy of Atlantic models was used here to investigate the different mechanisms causing interannual to decadal variability of the shallow subtropical-tropical cells (STCs). By utilizing a hierarchy of models of the basin-scale wind-driven and thermohaline circulation, using resolutions (1/3° and 1/12°) capable of depicting the main current features in the equatorial regime, the study can be regarded as building on, and extending the recent, regional model investigation by *Kröger et al.* [2005], particularly in two regards: by examining the spatial patterns of the STC variability, i.e., its manifestation in the western boundary (NBC) and equatorial (EUC) current systems; and by examining the contribution due to remotely forced changes in the deep MOC, i.e., the dynamical signals conveyed to the equatorial regime of subarctic MOC changes associated with the variability in LSW formation.

[52] Whereas comparisons between the eddy-permitting (1/3°-) and eddy-resolving (1/12°-model version) hindcast-

ing runs (Exp.1 and 2) exhibit substantial resolution dependencies in the details of the (intra-) seasonal transport variability, probably reflecting the impact of tropical instability waves [*Jochum et al.*, 2004], the lower-frequency variability characteristics appear rather robust. A remarkable robustness is particularly revealed in the zonally integrated STC variability, when comparing the patterns obtained in the main hindcasting experiment (Exp. 1) with the results reported for the regional, reduced-gravity model of *Kröger et al.* [2005]: the similarity between these two numerical models, which differ in many aspects of physical approximations (e.g., reduced-gravity versus primitive equations) and parameterizations, and use rather different concepts in the formulation of the atmospheric forcing (i.e., atmospheric mixed layer model versus linearized bulk formula for the air-sea heat fluxes) is strongly indicative of the overarching role of the local wind forcing (which in both cases is given by the NCEP/NCAR reanalysis data) in the generation of the decadal STC transport anomalies.

[53] The amplitude of the interannual-decadal variability in the zonally integrated STC transports is about 2 Sv in the 1/3°- and 1/12°- hindcasting experiments that are forced by both variable wind stresses and heat flux anomalies (Exps. 1 and 3, respectively). A sensitivity experiment (Exp. 3) in which the wind stresses were substituted by climatological, monthly mean values, indicates the maximum contribution of the heat flux variability to be of O(0.5 Sv): this contribution appears to manifest itself mainly as a low-frequency modulation of the transport time series, with a minimum in the upper-layer, northward transports in the early 1970s and a maximum in the mid-1990s. Aided by the signal propagation patterns obtained in the idealized response experiment (Exp. 4), the low-frequency signature in the hindcasted STC and NBC time series can be identified as a remote effect of changes in the North Atlantic's MOC associated with a heat flux-related variability in LSW formation. The fast propagation of subarctic transport anomalies to the equator was found to be close to previous studies [*Kawase*, 1987; *Johnson and Marshall*, 2002; *Getzlaff et al.*, 2005]. An idealized model setting by *Yang* [1999] dealt with the relative influence of LSW production on the tropical SST dipole: an O(10Sv) variation in LSW formation led to O(0.5°C) tropical dipole variability about 5 years later. A more recent analysis of *Bentsen et al.* [2004] corroborates the ideas of *Yang* [1999], showing a 6-year lag instead of 5-years in one of their experiments, but a dependence of the LSW-SST relation on the nature of air-sea coupling feedbacks which are not investigated here.

[54] The spatial patterns of the flow anomalies associated with the decadal STC variability show the highest velocity variance near the western boundary, along the NBC. An inspection of the relative contribution to the net, zonally integrated meridional transport variability reveals a more complicated picture: the fluctuations in the northward boundary current (the NBC) appear of similar magnitude as the integrated transports, but tend to show a reversed sign, i.e., a strengthening of the zonally integrated transport coincides with a weakening of the NBC transport. This behavior appears reminiscent of a similar situation that has been noted for the interannual to decadal scale variability in the Pacific STC transports [*Lee and Fukumori*, 2003; *Wang et al.*, 2003; *Capotondi et al.*, 2005], although, the mechanism of the out-of phase relation between interior and western boundary transport remains unclear. *Lee and Fukumori* [2003] explain the partial compensation of interior and boundary current transports due to the presence of two different mechanisms: while the boundary current variability results from the adjustment of the gyre circulation to changes in the Ekman pumping, the interior transport may also result from changes in the near-equatorial variations of surface wind stress. The results of *Capotondi et al.* [2005] suggest that both the western boundary and the interior transport are adjusted through baroclinic Rossby waves.

[55] An interesting aspect of the zonal distribution of the meridional transport anomalies is the different behavior between the wind-driven changes (the dominant signal in Exps. 1 and 2), and the changes associated with the MOC variability of subarctic origin (isolated in Exp. 3). While Exp. 1 shows a weak anti-correlation between zonally integrated STC and NBC south of 4°S and strong correlation equatorward of 4°S, Exp. 3 gave a high correlation (>0.6) between zonally integrated transport and boundary current transport over the latitude range between the equator and about 20°S. This suggests that thermohaline-driven signals, in contrast to wind-driven signals are primarily manifested in the (and confined to) the NBC. However, as the sensitivity runs (Exps. 3 and 4) indicate, the strength of the signal is small and difficult to detect in the much stronger wind-driven variability.

[56] **Acknowledgments.** This research was funded by the Bundesministerium fuer Bildung und Forschung (BMBF) as part of the German CLIVAR project (03F0377B). We acknowledge the contributions of the other members of the Kiel FLAME group to the development and integrations of the various model experiments used in this analysis. A significant part of the model development was accomplished as part of the SFB 460, funded by the Deutsche Forschungsgemeinschaft (DFG). The experiments have been performed using the facilities and services of the Deutsches Klimarechenzentrum (DKRZ), Hamburg. We also acknowledge the use of Ferret for analysis and graphics in this paper.

References

Barnier, B., et al. (1995), Thermal forcing for a global ocean circulation model using a three-year climatology of ECMWF analysis, *J. Mar. Syst.*, *6*, 363–380.

Barnier, B., T. Reynaud, A. Beckmann, C. Böning, J.-M. Molines, S. Barnard, and Y. Jia (2001), On the seasonal variability and eddies in the North Brazil Current: Insights from model intercomparison experiments, *Prog. Oceanogr.*, *48*, 195–230.

Beismann, J. O., and B. Barnier (2004), Variability fo the meridional overturning circulation of the North Atlantic: Sensitivity to the overflow of dense water masses, *Ocean Dyn.*, *54*(1), 701–720.

Bentsen, M., H. Drange, T. Furevik, and T. Zhou (2004), Simulated variability of the Atlantic meridional overturning circulation, *Clim. Dyn.*, *22*, 701–720.

Böning, C. W., and J. Kröger (2005), Seasonal variability of deep currents in the equatorial Atlantic: A model study, *Deep Sea Res.*, *52*(1), 99–121.

Böning, C. W., M. Rhein, J. Dengg, and C. Dorow (2003), Modeling CFC inventories and formation rates of Labrador Sea Water, *Geophys. Res. Lett.*, *30*(2), 1050, doi:10.1029/2002GL014855.

Bourles, B., R. L. Molinari, E. Johns, and W. Wilson (1999), Upper layer currents in the western tropical North Atlantic (1989–1991), *J. Geophys. Res.*, *104*(C1), 1361–1375.

Boyer, T. P., and S. Levitus (1997), Objective analyses of temperature and salinity for the world ocean on a 1/4 degree grid, technical report, NOAA Atlas NESDIS 11, U.S. Govt. Print. Off., Washington, D. C.

Brandt, P., and C. Eden (2005), Annual cycle and interannual variability of the mid-depth tropical Atlantic ocean, *Deep Sea Res.*, *52*(2), 199–219.

Capotondi, A. (2000), Oceanic wave dynamics and interdecadal variability in a climate system model, *J. Geophys. Res.*, *105*(C1), 1017–1036.

Capotondi, A., M. A. Alexander, C. Deser, and M. J. McPhaden (2005), Anatomy and decadal evolution of the Pacific Subtropical-Tropical Cells (STCs), *J. Clim.*, *18*(9), 3739–3758.

Carton, J. A., and B. Huang (1994), Warm events in the tropical Atlantic, *J. Phys. Oceanogr.*, *24*, 888–903.

Carton, J. A., X. Cao, B. S. Giese, and A. M. daSilva (1996), Decadal and interannual SST variability in the tropical Atlantic ocean, *J. Phys. Oceanogr.*, *26*, 1165–1175.

Chang, P., J. Link, and L. Hong (1997), A decadal climate variation in the tropical Atlantic ocean from thermodynamic air-sea interactions, *Nature*, *385*, 516–518.

Chang, P., L. Ji, and R. Saravanan (2001), A hybrid coupled model study of tropical Atlantic variability, *J. Clim.*, *14*(3), 361–390.

Curry, R. G., M. S. McCartney, and T. Joyce (1998), Oceanic transport of subpolar climate signals to mid-depth subtropical waters, *Nature*, *291*, 575–577.

Dommenget, D., and M. Latif (2000), Interannual to decadal variability in the tropical Atlantic, *J. Clim.*, *13*(4), 777–792.

Döscher, R., C. W. Böning, and P. Hermann (1994), Response of the circulation and heat transport in the North Atlantic to changes in thermohaline forcing in northern latitudes: A model study, *J. Phys. Oceanogr.*, *24*, 2306–2320.

Dynamo Group, (1997), *Dynamo Sci. Rep. 3*, Kiel, Germany.

Eden, C., and J. Willebrand (2001), Mechanism of interannual to decadal variability of the North Atlantic circulation, *J. Clim.*, *14*, 2266–2280.

Fratantoni, D., W. E. Johns, T. L. Townsend, and H. E. Hurlburt (2000), Low-latitude circulation and mass transport pathways in a model of the tropical Atlantic ocean, *J. Phys. Oceanogr.*, *30*(8), 1944–1966.

Ganachaud, A., and C. Wunsch (2001), Improved estimates of global ocean circulation, heat transport and mixing from hydrographical data, *Nature*, *408*, 453–457.

Getzlaff, J., C. W. Böning, C. Eden, and A. Biastoch (2005), Signal propagation related to the North Atlantic overturning, *Geophys. Res. Lett.*, *32*, L09602, doi:10.1029/2004GL021002.

Gouriou, Y., and G. Reverdin (1992), Isopycnal and diapycnal ciruclation of the upper equatorial Atlantic Ocean in 1983–1984, *J. Geophys. Res.*, *97*(C3), 3543–3572.

Gu, D., and S. G. H. Philander (1997), Interdecadal climate fluctuations that depend on exchanges between the tropics and the subtropics, *Science*, *275*, 805–807.

Häkkinen, S. (1999), A simulation of thermohaline effects of a Great Salinity Anomaly, *J. Clim.*, *12*(6), 1781–1795.

Hastenrath, S., and L. Greischar (1993), Further work on the prediction of northeast Brazil rainfall anomalies, *J. Clim.*, *6*, 743–758.

Hazeleger, W., P. de Vries, and Y. Friocourt (2003), Sources of the equatorial undercurrent in the Atlantic in a high resolution ocean model, *J. Phys. Oceanogr.*, *33*, 677–693.

Hisard, P. (1980), Observation de response de type El Nino dans l'Atlantique tropical oriental Golfe de Guinee, *Oceanol. Acta*, *3*, 69–78.

Inui, T., A. Lazar, P. Malanotte-Rizzoli, and A. Busalacchi (2002), Wind stress effects on subsurface pathways from the subtropical to tropical Atlantic, *J. Phys. Oceanogr.*, *32*(10), 2257–2276.

Jochum, M., and P. Malanotte-Rizzoli (2001), Influence of the meridional overturning circulation on tropical–subtropical pathways, *J. Phys. Oceanogr.*, *31*(5), 1313–1323.

Jochum, M., P. Malanotte-Rizzoli, and A. Busalacchi (2004), Tropical instability waves in the Atlantic ocean, *Ocean Modell.*, *7*, 146–163.

Johns, W. E., T. N. Lee, R. C. Beardsley, J. Candela, R. Limeburger, and B. Castro (1998), Annual cycle and variability of the North Brazil Current, *J. Phys. Oceanogr.*, *28*, 103–128.

Johnson, H. J., and D. P. Marshall (2002), A theory for the surface Atlantic response to thermohaline variability, *J. Phys. Oceanogr.*, *32*(4), 1121–1132.

Kalnay, E., et al. (1996), The NCEP 40-year reanalysis project, *Bull. Am. Meteorol. Soc.*, *77*, 437–471.

Kawase, M. (1987), Establishment of deep ocean circulation driven by deep-water production, *J. Phys. Oceanogr.*, *17*, 2294–2317.

Kleeman, R., J. P. McCreary, and B. A. Klinger (1999), A mechanism for generating ENSO decadal variability, *Geophys. Res. Lett.*, *26*(12), 1743–1746.

Kraus, E. B., and J. S. Turner (1967), A one–dimensional model of the seasonal thermocline I. a laboratory experiment and its interpretation, *Tellus*, *19*, 88–97.

Kröger, J. (2001), Mechanismen meridionaler Transportprozesse im tropischen Atlantik, Ph.D. thesis, Christian-Albrechts-Univ. zu Kiel, Kiel, Germany.

Kröger, J., A. Busalacchi, and J. Ballabrera-Poy (2005), Decadal variability of shallow cells and equatorial SST in a numerical model of the Atlantic, *J. Geophys. Res.*, *110*, C12003, doi:10.1029/2004JC002703.

Kushnir, Y., R. Seager, J. Miller, and J. C. H. Chiang (2002), A simple coupled model of tropical Atlantic decadal climate variability, *Geophys. Res. Lett.*, *29*(23), 2133, doi:10.1029/2002GL015874.

Lazar, A., R. Murtugudde, and A. J. Busalacchi (2001), A model study of temperature anomaly propagation from the subtropics to tropics within the South Atlantic thermocline, *Geophys. Res. Lett.*, *28*(7), 1271–1274.

Lazar, A., T. Inui, P. Malanotte-Rizzoli, A. J. Busalacchi, L. Wang, and R. Murtugudde (2002), Seasonality of the ventilation of the tropical Atlantic thermocline in an ocean general circulation model, *J. Geophys. Res.*, *107*(C8), 3104, doi:10.1029/2000JC000667.

Lee, T., and I. Fukumori (2003), Interannual-to-decadal variations of tropical-subtropical exchange in the Pacific ocean: Boundary versus interior pycnocline transports, *J. Clim.*, *16*, 4022–4042.

Levitus, S., and T. P. Boyer (1994), World ocean atlas 1994, NOAA Atlas NESDIS, Natl. Oceanic and Atmos. Admin., Washington D. C.

Liu, Z., S. G. H. Philander, and R. C. Pacanowski (1994), A GCM study of tropical-subtropical upper-ocean water exchange, *J. Phys. Oceanogr.*, *24*(12), 2606–2623.

Lu, P., J. P. McCreary, and B. A. Klinger (1998), Meridional circulation cells and the source waters of the Pacific equatorial undercurrent, *J. Phys. Oceanogr.*, *28*(1), 62–84.

Lumpkin, R., and K. Speer (2003), Large-scale vertical and horizontal circulation in the North Atlantic ocean, *J. Phys. Oceanogr.*, *33*(9), 1902–1920.

Malanotte-Rizzoli, P., K. Hedstrom, H. Arango, and D. B. Haidvogel (2000), Water mass pathways between the subtropical and tropical ocean in a climatological simulation of the North Atlantic ocean circulation, *Dyn. Atmos. Oceans*, *32*, 331–371.

Marsh, R. (2000), Recent variability of the North Atlantic thermohaline circulation inferred from surface heat and freshwater fluxes, *J. Clim.*, *13*(18), 3239–3260.

McCreary, J. P., and P. Lu (1994), Interaction between the subtropical and equatorial ocean circulations: The subtropical cell, *J. Phys. Oceanogr.*, *24*(2), 466–497.

McPhaden, M. J., and D. Zhang (2002), Slowdown of the meridional overturning circulation in the upper Pacific ocean, *Nature*, *415*, 603–608.

Metcalf, W., and M. C. Stalcup (1967), Origin of the Atlantic equatorial undercurrent, *J. Geophys. Res.*, *72*(20), 4959–4975.

Molinari, R. L., S. Bauer, D. P. Snowden, G. C. Johnson, B. Bourles, Y. Gouriou, and H. Mercier (2004), A comparision of kinematic evidence for tropical cells in the Atlantic and Pacific oceans, in *Interhemispheric Water Exchanges in the Atlantic Ocean*, *Elsevier Oceanogr. Ser.*, Elsevier, New York.

Nonaka, M., S. P. Xie, and J. P. McCreary (2002), Decadal variations in the subtropical cells and equatorial Pacific SST, *Geophys. Res. Lett.*, *29*(7), 1116, doi:10.1029/2001GL013717.

Oschlies, A., and V. Garcon (1999), An eddy-permitting coupled physical-biological model of the North Atlantic: 1. Sensitivity to advection numerics and mixed layer physics, *Global Biogeochem. Cycles*, *13*, 135–160.

Pacanowski, R. C. (1995), MOM 2 Documentation, User's Guide and Reference Manual, *Tech. Rep. 3*, Ocean Group, Geophys. Fluid Dyn. Lab., Princeton, N. J.

Philander, S. G. H., and R. C. Pacanowski (1986), A model of the seasonal cycle in the tropical Atlantic Ocean, *J. Geophys. Res.*, *91*(C12), 14,192–14,206.

Rhein, M., J. Fischer, W. M. Smethie, D. Smythe-Wright, R. F. Weiss, C. Mertens, D.-H. Min, U. Fleischmann, and A. Putzka (2002), Labrador Sea Water: Pathways, CFC inventory and formation rates, *J. Phys. Oceanogr.*, *32*(2), 648–665.

Schott, F., M. Dengler, P. Brandt, K. Affler, J. Fischer, B. Bourles, Y. Gouriou, R. L. Molinari, and M. Rhein (2003), The zonal currents and transports at 35°W in the tropical Atlantic, *Geophys. Res. Lett.*, *30*(7), 1349, doi:10.1029/2002GL016849.

Schott, F., M. Dengler, R. Zantopp, L. Stramma, J. Fischer, and P. Brandt (2005), The shallow and deep western boundary circulation of the south Atlantic at 5-11S, *J. Phys. Oceanogr.*, *35*, 2031–2053.

Schott, F. A., and C. W. Böning (1991), The WOCE model in the western equatorial Atlantic: Upper layer circulation, *J. Geophys. Res.*, *96*(C4), 6993–7004.

Schott, F. A., J. Fischer, and Stramma (1998), Transports and pathways of the upper–layer circulation in the western tropical Atlantic, *J. Phys. Oceanogr.*, *28*, 1904–1928.

Schott, F. A., P. Brandt, M. Hamann, J. Fischer, and L. Stramma (2002), On the boundary flow off Brazil at 5–10°s and its connection to the interior tropical Atlantic, *Geophys. Res. Lett.*, *29*(17), 1840, doi:10.1029/2002GL014786.

Schott, F. A., J. P. McCreary, and G. Johnson (2004), Shallow overturning circulations of the tropical-subtropical oceans, in *Earth Climate: The*

Ocean-Atmosphere Interactions, *Geophys. Monogr. Ser.*, vol. 147, pp. 261–304, AGU, Washington, D. C.

Seager, R., Y. Kushnir, P. Chang, N. H. Naik, J. Miller, and W. Hazeleger (2001), Looking for the role of the ocean in tropical Atlantic decadal climate variability, *J. Clim.*, *14*(5), 638–655.

Stramma, L., S. Hüttl, and J. Schafstall (2005a), Water masses and currents in the upper tropical northeast Atlantic off northwest Africa, *J. Geophys. Res.*, *110*, C12006, doi:10.1029/2005JC002939.

Stramma, L., M. Rhein, P. Brandt, M. Dengler, C. Böning, and M. Walter (2005b), Upper ocean circulation in the western tropical Atlantic in boreal fall 2000, *Deep Sea Res.*, *52*(1), 221–240.

Thierry, V., A. M. Treguier, and H. Mercier (2004), Numerical study of the annual and semi-annual fluctuations in the deep equatorial Atlantic ocean, *Ocean Modell.*, *6*, 1–30.

Tsuchiya, M. (1986), Thermostads and circulation in the upper layer of the Atlantic ocean, *Prog. Oceanogr.*, *16*, 235–267.

Wang, X. C., F. F. Jin, and Y. Q. Wang (2003), A tropical ocean recharge mechanism for climate variability, Part II: A unified theory for decadal and ENSO modes, *J. Clim.*, *16*, 3585–3598.

Willebrand, J., B. Barnier, C. Böning, C. Dieterich, P. D. Killworth, C. LeProvost, Y. Jia, J.-M. Molines, and A. L. New (2001), Circulation characteristics in three eddy–permitting models of the North Atlantic, *Prog. Oceanogr.*, *48*, 123–161.

Wilson, W. D., E. Johns, and R.-L. Molinari (1994), Upper layer circulation in the western tropical North Atlantic Ocean during August 1989, *J. Geophys. Res.*, *99*(C11), 22,513–22,523.

Yang, J. (1999), A linkage between decadal climate variations in the Labrador Sea and the tropical Atlantic Ocean, *Geophys. Res. Lett.*, *26*(8), 1023–1026.

Zhang, D., M. J. McPhaden, and W. E. Johns (2003), Observational evidence for flow between the subtropical and tropical Atlantic: the Atlantic subtropical cells, *J. Phys. Oceanogr.*, *33*(8), 1783–1797.

Zhang, R., and T. L. Delworth (2005), Simulated tropical response to a substantial weakening of the Atlantic thermohaline circulation, *J. Clim.*, *18*(6), 1853–1860.

C. W. Böning and S. Hüttl, Leibniz-Institut für Meereswissenschaften an der Universität Kiel, IFM-GEOMAR, Düsternbrooker Weg 20, D-24105 Kiel, Germany. (shuettl@ifm-geomar.de)